Quaternary Science Reviews 173 (2017) 1–19

Contents lists available at ScienceDirect

Quaternary Science Reviews

journal homepage: www.elsevier.com/locate/quascirev

Invited review

Constraining processes of landscape change with combined *in situ* cosmogenic ^{14}C-^{10}Be analysis

Kristina Hippe

Laboratory of Ion Beam Physics, ETH Zürich, Otto-Stern-Weg 5, CH-8093 Zürich, Switzerland

ARTICLE INFO

Article history:
Received 11 April 2017
Received in revised form
26 July 2017
Accepted 28 July 2017

Keywords:
Cosmogenic nuclides
Quaternary
Surface exposure dating
Complex exposure
Glacial
Inheritance
Sediment
Soil
Erosion

ABSTRACT

Reconstructing Quaternary landscape evolution today frequently builds upon cosmogenic-nuclide surface exposure dating. However, the study of complex surface exposure chronologies on the 10^2–10^4 years' timescale remains challenging with the commonly used long-lived radionuclides (^{10}Be, ^{26}Al, ^{36}Cl). In glacial settings, key points are the inheritance of nuclides accumulated in a rock surface during a previous exposure episode and (partial) shielding of a rock surface after the main deglaciation event, e.g. during phases of glacier readvance. Combining the short-lived *in situ* cosmogenic ^{14}C isotope with ^{10}Be dating provides a valuable approach to resolve and quantify complex exposure histories and burial episodes within Lateglacial and Holocene timescales. The first studies applying the *in situ* ^{14}C-^{10}Be pair have demonstrated the great benefit from *in situ* ^{14}C analysis for unravelling complex glacier chronologies in various glacial environments worldwide. Moreover, emerging research on *in situ* ^{14}C in sedimentary systems highlights the capacity of combined *in situ* ^{14}C-^{10}Be analysis to quantify sediment transfer times in fluvial catchments or to constrain changes in surface erosion rates. Nevertheless, further methodological advances are needed to obtain truly routine and widely available *in situ* ^{14}C analysis. Future development in analytical techniques has to focus on improving the analytical reproducibility, reducing the background level and determining more accurate muonic production rates. These improvements should allow extending the field of applications for combined *in situ* ^{14}C-^{10}Be analysis in Earth surface sciences and open up a number of promising applications for dating young sedimentary deposits and the quantification of recent changes in surface erosion dynamics.

1. Introduction

The development of surface exposure dating with cosmogenic nuclides has opened up new perspectives for Quaternary geochronology and revolutionized our ability to constrain landscape history (e.g., Balco, 2011; von Blanckenburg and Willenbring, 2014). In glacial landscapes, cosmogenic-nuclide surface exposure dating provides a unique method to directly date the formation of glacial landforms, e.g. the deposition of moraines or erratic boulders, as well as the time of disappearance of glacier ice from a bedrock surface (Ivy-Ochs and Briner, 2014). Cosmogenic nuclides have become an integral part of quantitative geomorphology and are one of the most widely used tools to determine the deposition age of sedimentary landforms and volcanic deposits, to reconstruct paleoearthquake activity and to quantify local to landscape-wide soil-formation and hillslope erosion dynamics (for reviews see e.g., Cerling and Craig, 1994; Gosse and Phillips, 2001; Dunai, 2010; Granger et al., 2013). The principle of cosmogenic-nuclide surface exposure dating is based on the production of cosmogenic isotopes within the uppermost few meters of the Earth surface by interaction of secondary cosmic-ray particles with atoms in the rocks (Dunai, 2010). The concentration of a cosmogenic nuclide primarily depends on the time since initial exposure to cosmic rays, the rate of its production, and the rate of its removal by radioactive decay or erosion (Gosse and Phillips, 2001). A number of stable (^3He, ^{21}Ne) and radioactive cosmogenic nuclides (^{10}Be, *in situ* ^{14}C, ^{26}Al, ^{36}Cl) are currently used to study Earth surface evolution, with ^{10}Be being the most widely applied nuclide. *In situ* ^{14}C sticks out of the list of cosmogenic nuclides by its short half-life of only 5700 ± 30 years (www.nndc.bnl.gov, National Nuclear Data Center) compared to the much longer half-lives of 1.4 Ma, 0.7 Ma and 0.3 Ma for ^{10}Be, ^{26}Al and ^{36}Cl, respectively. Because of its fast decay, the *in situ* ^{14}C concentration will rapidly decrease as soon as a bedrock, sediment or soil surface is shielded from cosmic rays by being covered under several meters of sediment, soil or ice. This means that *in situ* ^{14}C,

E-mail address: hippe@phys.ethz.ch.

http://dx.doi.org/10.1016/j.quascirev.2017.07.020
0277-3791/

when paired with a long-lived nuclide, allows detecting complex surface exposure histories caused by interruptions in surface exposure (e.g. by glacier readvance) or sediment transport, changes in surface erosion rates or events of mass removal within Holocene to latest Pleistocene timescales.

This review paper provides an introduction to *in situ* cosmogenic ^{14}C dating, particularly in combination with ^{10}Be, and present the hitherto few applications of coupled *in situ* ^{14}C-^{10}Be analysis. It outlines the development and present status of *in situ* ^{14}C analytical techniques and discusses the current challenges with regard to analytical reliability and the accuracy of production rates. Although *in situ* ^{14}C extraction methods and protocols that have set the foundation for the currently applied techniques were developed during the 1990s (e.g., Jull et al., 1992; Lifton et al., 2001), *in situ* ^{14}C extraction from terrestrial rocks is still a technically challenging process that is not yet widely employed. Consequently, the number of publications reporting *in situ* ^{14}C data remains limited. So far, the quantification of complex surface exposure histories in landscapes previously or still covered by glaciers has been the primary application for *in situ* ^{14}C analysis, with a total of ten papers published since 2006. This trend can be partially related to the comparatively straightforward interpretation of *in situ* ^{14}C data from glacially modified surfaces (in contrast to, e.g., *in situ* ^{14}C in sediments), the insensitivity of *in situ* ^{14}C to surface pre-exposure and its high sensitivity to post-exposure surface shielding. Besides glacier chronologies, this review will further discuss the potential of *in situ* ^{14}C analysis for quantifying surface processes and landscape evolution outside glacial settings. The aim is to describe the conceptual framework and to outline the direction of improvements needed to exploit the full potential of *in situ* ^{14}C in Quaternary geochronology and Earth surface process dating.

2. Principles of *in situ* ^{14}C production

2.1. Production mechanisms

In the 1940s the development of radiocarbon analysis introduced the ^{14}C isotope as a geochronological tool for dating organic material (Libby, 1946; Anderson et al., 1947; Libby et al., 1949). In conjunction with the huge progress made on AMS techniques (Jull and Burr, 2006 and references therein), radiocarbon dating quickly became one of the most widely used Quaternary dating methods. However, it was soon recognized that the ^{14}C isotope is not only produced by cosmic-ray interactions in the atmosphere but also at the solid Earth surface, i.e. *"in situ"* (Lal and Peters, 1967).

In situ ^{14}C is produced by the same production pathways as the long-lived cosmogenic ^{10}Be and ^{26}Al nuclides, i.e. by the collision of secondary cosmic-ray particles (neutrons and muons) with atoms in rocks at the Earth's surface (e.g., Lal, 1988; Heisinger and Nolte, 2000; Gosse and Phillips, 2001; Dunai, 2010). Nuclide production is dominated by spallation reactions caused by highly energetic neutrons. For *in situ* ^{14}C, the primary target for spallation reactions is O (^{16}O(n, 2pn)^{14}C, ^{17}O(n, α)^{14}C); minor production occurs from Si, Mg, and Al (Dunai, 2010). Further production occurs by interactions with low-energy muon particles, either by negative muon capture or by neutron reactions induced by fast muons (Heisinger et al., 2002a,b). While production by spallation decreases exponentially with depth below the surface (Fig. 1), muons can penetrate deeper into the subsurface due to their much larger attenuation lengths compared to neutrons. Below a few meters depth (about 3–4 m of rock or ~1000 g cm^{-2}), muonic processes overtake spallogenic processes and dominate nuclide production. Therefore, the magnitude of muonic production is most important for applications that require an accurate estimate of nuclides produced at depth. These include the quantification of surface erosion rates (especially for fast eroding landscapes), dating of erosional surfaces by depth profiles as well as paired-nuclide burial dating, and the calculation of post-burial nuclide production in surfaces or sediment deposits that have not been completely shielded from the cosmic-ray flux. The muon contribution to the total *in situ* ^{14}C surface production rate (at sea level high latitude = SLHL) is estimated at >20% (Lupker et al., 2015) which is considerably higher than the ~1.5–2% of muon contribution to the surface production rates of ^{10}Be or ^{26}Al (Borchers et al., 2016). Due to this large muon component, all applications involving *in situ* ^{14}C analysis need to accurately account for muonic ^{14}C production rates including an appropriate estimate for muonic production in the subsurface (for a detailed discussion see Balco, 2017).

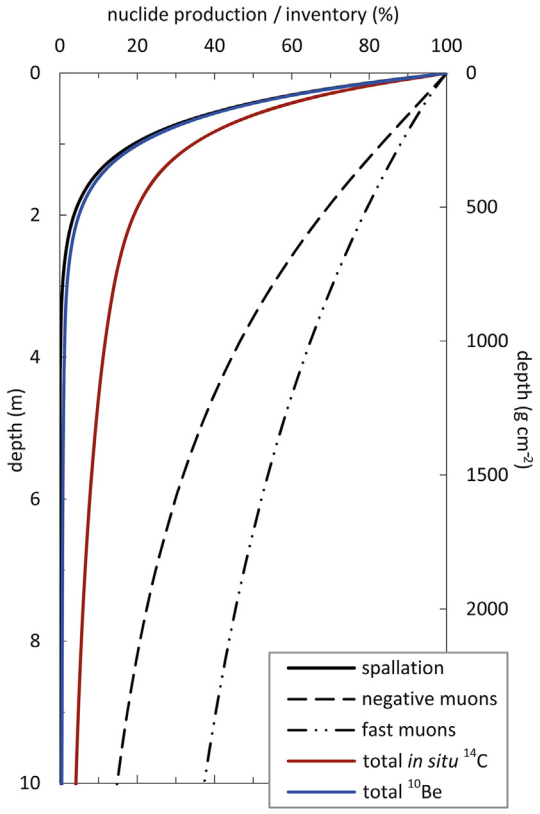

Fig. 1. Relative nuclide production or nuclide inventory, respectively, of *in situ* ^{14}C and ^{10}Be at depth below the surface, calculated for a rock density of $\rho = 2.65$ g cm^{-3}. Black solid line illustrates the decrease in the spallation production rate (or nuclide concentration), dashed and dot-dashed lines refer to negative muon capture and fast muon processes, respectively. Calculated for SLHL with spallogenic production rates (Lm scaling) of 4.00 ± 0.32 at g^{-1} a^{-1} for ^{10}Be and 12.2 ± 0.89 at g^{-1} a^{-1} for *in situ* ^{14}C (Phillips et al., 2016a). Depth dependence for spallation follows an exponential decrease. Muonic nuclide production at depth was calculated with the freely available MATLAB code from the online calculator (v. 2.3) of Balco et al. (2008b) using updated muon interaction cross-sections as given in Borchers et al. (2016) for ^{10}Be and muon cross-sections of Heisinger et al. (2002a,b) for *in situ* ^{14}C.

2.2. Production rates

Since the accuracy of any cosmogenic nuclide exposure age critically depends on the accurate knowledge of the production rate of each specific nuclide, production rate determination and site-specific scaling represent a highly important issue for the cosmogenic nuclide community. Over the past 10 years many researchers – independently or in connection with the CRONUS-Earth and CRONUS-EU projects (Stuart and Dunai, 2009; Phillips et al., 2016b) – have dedicated significant effort to improve the understanding of

cosmogenic nuclide production and produce widely-accepted and internally consistent calibration datasets to reduce the uncertainties on the production rates of all commonly used cosmogenic nuclides.

The most recent estimate for the *in situ* ^{14}C spallation production rate in quartz is based on ~90 analyses from six calibration sites and yields a SLHL value of 12.76 at g^{-1} a^{-1} for the new LSD (or Sa) scaling (Borchers et al., 2016; Phillips et al., 2016a) which equals a SLHL rate of 12.24 at g^{-1} a^{-1} for the so far predominantly used St scaling method (Lal, 1991; Stone, 2000). An uncertainty of 7.3% was assumed for the new production rate estimate but could not be validated by the statistical χ^2 test due to a large scatter of the *in situ* ^{14}C data (Borchers et al., 2016). The revised production rate does not include the previously published production rate data reported from Lake Bonneville (Utah, USA), the Scottish Highlands, the Southern Alps of New Zealand and West Greenland (summarized in Schimmelpfennig et al., 2012; Young et al., 2014). However, it is in good agreement with these earlier calibration data.

The calculation of *in situ* ^{14}C production from muon reactions has so far been based on the model and parameters specified by Heisinger et al. (2002a,b). These authors experimentally determined muon interaction cross-sections and calculated the rates and depth dependence of muonic nuclide production. *In situ* ^{14}C SLHL muonic production rates given by Heisinger et al. (2002a,b) are 3.34 ± 0.27 at g^{-1} a^{-1} for negative muon capture and 0.44 ± 0.25 at g^{-1} a^{-1} for fast muon reactions. Compared to ^{10}Be or ^{26}Al, only little *in situ* ^{14}C data is available from analyses of natural depth profiles. *In situ* ^{14}C concentrations measured by Kim et al. (2007) to a depth of 1.45 m at Macraes Flat (New Zealand) did not allow a quantification of muonic production rates due to exceptionally high ^{14}C concentrations. A first estimate of *in situ* ^{14}C muonic production from a natural setting was recently presented by Lupker et al. (2015) who reported *in situ* ^{14}C concentrations measured in a quartzite core at Leymon High (Spain) to a depth of 15.5 m. Based on these data, muonic production rates for SLHL and Lal/Stone scaling of 3.31 (+0.43/-1.07) at g^{-1} a^{-1} for negative muon capture and 0 (+0.42/-0.00) at g^{-1} a^{-1} for fast muon reactions were modelled (Lupker et al., 2015). These values are in good agreement with the experimental results of Heisinger et al. (2002a,b) and confirm the comparatively large contribution of muon components (~23%) to the total surface *in situ* ^{14}C production. In a careful re-evaluation of existing ^{10}Be, ^{26}Al and *in situ* ^{14}C muon data, Balco (2017) reproduced the results of Lupker et al. (2015) using a slightly different modelling approach to recalculate muonic production at depth. As pointed out by Lupker et al. (2015), the distinction of the fast muon component from the negative muon capture processes is particularly difficult as even at 15 m depth fast muon reactions only account for ~30% of the total muonic production. A better resolution of the fast muon contribution necessitates *in situ* ^{14}C measurements from greater depths where the relative amount of fast muon reactions is higher. However, measuring the extremely low *in situ* ^{14}C concentrations at great depths is limited by the current analytical capabilities.

2.3. Production-rate scaling

Since the incoming cosmic ray flux is partially shielded by the Earth magnetic field and is further attenuated through interactions with the Earth atmosphere, cosmogenic nuclide production rates need to be scaled to the geographic location (e.g., Lal and Peters, 1967; Lal, 1991). Production rate scaling as a function of latitude (or geomagnetic cutoff rigidity) accounts for the shielding effect by variations in the magnetic field that is stronger at low latitude and weakest at the poles. However, the geomagnetic shielding effect also varied in time due to fluctuations in the geomagnetic field intensity (Gosse and Phillips, 2001; Masarik et al., 2001; Lifton et al., 2008). The influence of magnetic field fluctuations on the cosmogenic nuclide production rates is most important for young exposure ages. With increasing exposure time the effect is averaged out and gets largely insignificant for ages ≥40 ka (Masarik et al., 2001). As *in situ* ^{14}C dating is confined to Holocene and Late Pleistocene timescales, geomagnetic field effects on the calculation of the time-integrated production rate have to be taken into account to obtain accurate *in situ* ^{14}C exposure ages. Correction for geomagnetic field fluctuations are accomplished in different production rate scaling models (Lal, 1991; Dunai, 2001a; Desilets and Zreda, 2003; Lifton et al., 2005, 2008, 2014) that are also implemented in the online calculators presently available to calculate surface exposure ages or erosion rates from cosmogenic nuclide data, i.e. the online calculator of Balco et al. (2008b; http://hess.ess.washington.edu/math/), CRONUScalc (Marrero et al., 2016; http://web1.ittc.ku.edu:8888/2.0/), CREp (Martin et al., 2017; http://crep.crpg.cnrs-nancy.fr) and the ICE-D database (http://antarctica.ice-d.org/).

Production rate scaling as a function of altitude accounts for the increasing abundance of cosmic-ray particles with decreasing atmospheric depth. Because the attenuation of particles in the atmosphere depends on the particle's energy, nuclide production by high-energy spallation reactions increases much stronger with altitude than lower-energy muon interactions (cf. Lal, 1991; Dunai, 2001b; Desilets and Zreda, 2003; Desilets et al., 2006). Therefore, an independent altitude scaling for spallogenic and muonic processes is needed to obtain accurate site-specific total production rates. Another aspect in connection with *in situ* ^{14}C production rate scaling is the question of nuclide specific variations in production rates. Today, the same production rate scaling methods are applied for all studied cosmogenic nuclides disregarding differences in the individual nuclide cross sections that are relevant for the production of each nuclide (Caffee et al., 2013; Reedy, 2013). However, production rate modelling proposes deviations in the ^{14}C/^{10}Be production ratio with increasing altitude that can amount to ~5% for altitudes around 4000 m compared to the sea level ^{14}C/^{10}Be production ratio (Argento et al., 2015a,b). In effect, these discrepancies will be small for most applications but might have to be considered in studies using the *in situ* ^{14}C-^{10}Be pair at high elevation sites.

3. *In situ* ^{14}C analytical methods

3.1. Historical development

The first measurements of the *in situ* ^{14}C content of whole rocks were obtained by pyrolysis of meteorites (Goel and Kohman, 1962; Suess and Wänke, 1962) to determine their terrestrial ages (the fall age) (Cresswell et al., 1994 and references therein). Because the ^{14}C concentration in extra-terrestrial material is usually over two orders of magnitude higher than in terrestrial rocks (Lal and Peters, 1967; Lifton et al., 2001) it can be more easily determined for meteorites. Early experiments on the *in situ* ^{14}C content in terrestrial rocks (basalts) employed sequential sample combustion (Desmarais, 1978a) followed by isolation of CO_2 by distillation at variable temperature traps (Desmarais, 1978b; Desmarais and Moore, 1984). In a similar approach, at the University of Arizona *in situ* ^{14}C extraction was performed on few grams of whole rock samples that were fused with an iron combustion flux in a flow of oxygen (Jull et al., 1989). This protocol also included a pre-heating step at 500 °C to remove atmospheric contaminants. To compensate for the low *in situ* ^{14}C concentration in terrestrial rocks, first analyses focussed on high-altitude samples that were at or close to saturation (Jull et al., 1989, 1992). The extraction procedure was

subsequently refined using larger sample sizes, a more rigorous chemical pre-cleaning of the sample and longer heating times (Jull et al., 1994). However, large and variable procedural blanks on the order of 10^6 ^{14}C atoms and variable ^{14}C yields remained major obstacles for routine *in situ* ^{14}C analysis from terrestrial rocks (Jull et al., 1994).

An alternative technique for *in situ* ^{14}C extraction used wet sample digestion with hydrofluoric acid (HF). This method relies on the separation of ^{14}CO and $^{14}CO_2$ in order to isolate the atmospheric ^{14}C from the *in situ* produced component (Cresswell et al., 1993, 1994; Lal and Jull, 1994). However, due to highly variable initial $^{14}CO/^{14}CO_2$ ratios in quartz and partial conversion of CO into CO_2 in the digestion process this approach has not been pursued any further (Lal and Jull, 2001; Kim et al., 2007). Besides silicates being the main target for *in situ* ^{14}C analysis, Handwerger et al. (1999) reported *in situ* ^{14}C extraction from carbonates using acidic sample dissolution with phosphoric acid (H_3PO_4).

3.2. Current techniques and abilities

Following the approach of stepwise sample combustion but redesigning the extraction system and modifying the analytical protocol, Lifton et al. (2001) presented an improved extraction procedure developed at U. Arizona. Whole-rock analysis was entirely given up in favour of purified quartz samples. The modified extraction system increased the reproducibility and showed more stable blank values in the lower range of 10^5 ^{14}C atoms (Lifton et al., 2001). It was further simplified in the following years (Pigati et al., 2010) and subsequently served as a prototype and model for a number of *in situ* ^{14}C extraction lines established at other facilities (Naysmith et al., 2004; Yokoyama et al., 2004; Hippe et al., 2009, 2013b; Fülöp et al., 2010, 2015b; Goehring et al., 2014; Lifton et al., 2015; Kim et al., 2016). While not all of these systems have reported ongoing operation, a few new extraction lines are currently under construction.

Probably the most important difference among the present *in situ* ^{14}C extraction lines lies in the method of sample combustion. On the one hand, *in situ* ^{14}C can be released from quartz by sample melting. This is achieved at 1100 °C with the addition of $LiBO_2$ (lithium metaborate) as a flux agent (e.g., Lifton et al., 2001, 2015; Goehring et al., 2014). The use of a flux has the advantage of comparatively low operating temperatures that can be easily reached and maintained for several hours by relatively inexpensive, off-the-shelf resistance furnaces. To remove carbon contamination the $LiBO_2$ needs to be fused and degassed at extraction temperatures prior to its addition to the quartz sample. However, some contamination remains from the $LiBO_2$. An alternative is the solid-state extraction of *in situ* ^{14}C by diffusion at temperatures >1500 °C (Lifton et al., 2001; Yokoyama et al., 2004). As a result of the phase transformation from quartz to cristobalite above 1470 °C the crystal lattice undergoes restructuring that releases the trapped carbon (Navrotsky, 1994). This approach allows obtaining *in situ* ^{14}C extraction without a flux agent by heating for 2–5 h to temperatures of 1550–1650 °C (Hippe et al., 2009; Fülöp et al., 2015b). The clear advantage is the omission of the flux as a major source of contamination. However, the high operating temperatures imply more sophisticated and costly extraction furnaces.

Although the few existing extraction systems use slightly variable procedures, in general the extraction of *in situ* ^{14}C from quartz is based on several common analytical steps (Fig. 2): (i) preparation of purified quartz through acid leaching and other mineral separation techniques, (ii) sample pre-heating at 500 °C (1–2 h) to remove atmospheric ^{14}C adsorbed to the crystal surfaces, (iii) release of the *in situ* component through heating to high temperatures for several hours (i.e., 1100 °C vs. 1550–1650 °C for flux vs. non-flux systems), (iv) oxidation of all carbon species into CO_2 to avoid the uncertainties of a poorly known $^{14}CO/^{14}CO_2$ ratio, (v) gas purification by cryogenic sublimation and passage through hot Cu (+Ag), (vi) and measurement of the extracted amount of CO_2 prior to sample transfer to an accelerator mass spectrometry (AMS) facility. Commonly, CO_2 gas samples are graphitized prior to AMS measurement which requires the addition of ^{14}C-free ("dead") CO_2. However, at ETH Zürich CO_2 can also be measured in the gas phase using the gas ion source of the MICADAS AMS system (Ruff et al., 2007; Synal et al., 2007). This speeds up sample processing and avoids additional contamination from the graphitization process. Due to the necessary pre-cleaning for sample holders and flux agent, sample pre-heating to remove atmospheric contamination and the required pump-down times between the individual procedural steps, extraction of *in situ* ^{14}C from quartz is a time-consuming procedure that has so far taken about two days per sample at most facilities. A recently introduced extraction scheme that is heating up to three tube-sealed samples at the same time in one extraction furnace, promises increased sample throughput of up to two samples per day (Fülöp et al., 2015b).

AMS measurements for *in situ* ^{14}C usually follow identical procedures as analyses of ^{14}C extracted from organic material. This includes a normalization of the measured $^{14}C/^{12}C$ ratio to AD 1950 ("pre-bomb" atmospheric ^{14}C) and to $\delta^{13}C = -25‰$ for isotopic fractionation. However, since anthropogenic changes in the atmospheric ^{14}C composition or fractionation processes during ^{14}C uptake in organic matter do not influence the production of *in situ* ^{14}C in quartz, AMS data reduction does not require these normalizations and data reporting for *in situ* ^{14}C has to be adjusted accordingly (Hippe and Lifton, 2014).

3.3. Blanks and detection limits

Analyses to determine the procedural blank apply the full extraction procedure as done for a quartz sample but either using ^{14}C-free quartz (synthetic or natural) or without adding any quartz into the system. Procedural blanks reported for flux-based extraction systems are on the order of ~$1–2 \cdot 10^5$ ^{14}C atoms, both for quartz-free blanks (Pigati et al., 2010; Schimmelpfennig et al., 2012; Goehring et al., 2014; Lifton et al., 2015) and for blanks using quartz from rocks that have been shielded from the cosmic-ray flux (Fülöp et al., 2010). Analytical uncertainties for the mean blank values reported from the different laboratories are on the order of 10–35% (1σ) which reflects the AMS statistical errors on the individual blank analyses and is in the same range as the overall scatter of the blank results. For flux-free systems, procedural blanks are about one order of magnitude lower than for flux-based systems. Procedural blanks of ~$1–4 \cdot 10^4$ ^{14}C atoms have been reported for blank analyses without (Hippe et al., 2013b; Lupker et al., 2015) as well as with quartz addition (Fülöp et al., 2015b). Associated uncertainties for the mean blank values are comparatively high and range from 60 to 160% (1σ). These uncertainties mainly record the large scatter in the obtained blank data. For example, procedural blanks reported by Lupker et al. (2015) were measured with AMS uncertainties of on average well below 10% but yield a standard deviation of up to ~60%.

Fig. 3 illustrates the dependency of the AMS counting uncertainty and the total analytical uncertainty, respectively, on the *in situ* ^{14}C concentration of a measured quartz sample (for sample sizes of 5 g qtz). Given data represent *in situ* ^{14}C from natural quartz ($n = 110$) of sedimentary and igneous origin that was extracted and measured at ETH Zürich over about a 2-year interval. The data show a significant increase in the total uncertainty (AMS counting error plus blank correction) for ^{14}C concentrations below $1 \cdot 10^5$ at g^{-1} which is in agreement with previous observations by Goehring

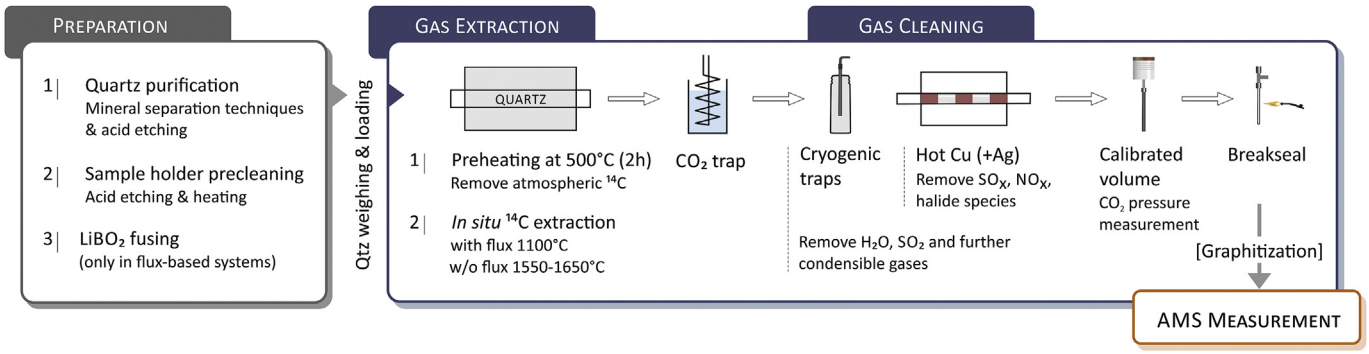

Fig. 2. Simplified procedure for the extraction of *in situ* ^{14}C from quartz. The diagram illustrates the key steps that are common to all currently running *in situ* ^{14}C extraction systems. In most laboratories, gas extraction is performed under addition of oxygen to ensure oxidation of all released carbon species into CO_2 (Lifton et al., 2001, 2015; Fülöp et al., 2010; Pigati et al., 2010; Hippe et al., 2013b; Goehring et al., 2014). The procedures applied for gas cleaning, i.e. the isolation of CO_2 from other contaminant gases, vary between the different laboratories with regard to the number and temperatures of cryogenic traps as well as the order in which the individual cleaning steps are performed. Please note that prior to the transfer of the sample to the AMS facility ^{14}C-free CO_2 might be added to ensure that the gas amount is large enough for the AMS measurement. Transformation of the CO_2 gas into graphite is not needed for AMS systems equipped with a gas ion source. Determining the amount of released CO_2 is required to calculate an absolute *in situ* ^{14}C concentration from the $^{14}C/^{12}C$ ratio measured by AMS.

et al. (2014) for *in situ* ^{14}C data from the Lamont-Doherty Earth Observatory. Concentrations of ~ $1–2 \cdot 10^5$ at g^{-1} seem to represent a threshold below which relative uncertainties increase and above which they remain on a more or less constant level (on average < 2% total uncertainty). This threshold marks the shift from the dominance of AMS counting errors at high concentrations towards the dominance in blank correction at lower concentrations. Uncertainties for AMS counting statistics increase only moderately and remain well below 10%, mostly below 5%, even for concentrations in the lower 10^4 at g^{-1} range. In contrast, blank corrections primarily control the rapid increase in the total uncertainty towards low concentrations. For illustration, an *in situ* ^{14}C concentration of ~$5 \cdot 10^4$ at g^{-1} corresponds to surface exposure at SLHL of about 320 years.

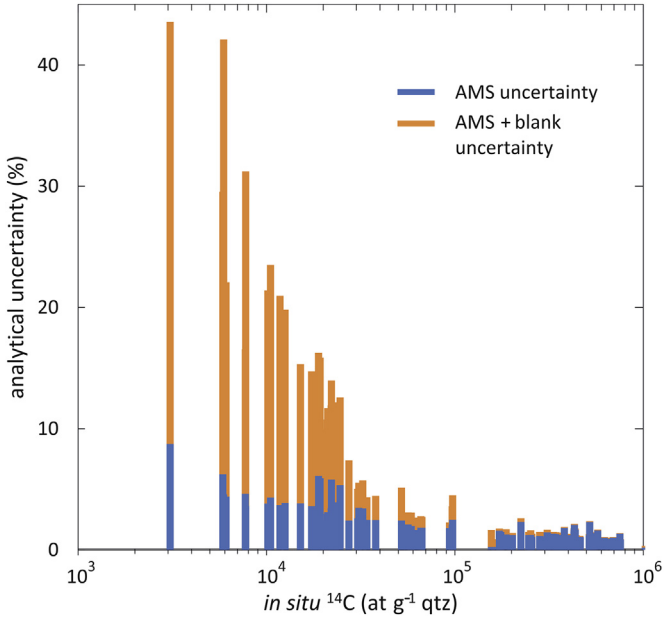

Fig. 3. *In situ* ^{14}C sample concentration vs. the analytical uncertainty, given for natural quartz samples (n = 110) measured at ETH Zürich during 2010–2012. The blue data show the analytical uncertainty obtained from the AMS measurement only (including small contributions from uncertainties on the determination of the extracted the CO_2 and a possible addition of ^{14}C-free CO_2). The orange data show the total analytical uncertainty as the sum of the AMS counting errors and uncertainties related to the blank correction. Minor scatter in the diagram is attributed to the fact that the values applied for blank corrections and their associated uncertainties varied over the 2-year time span. However, this does not affect the overall trend in the data.

In summary, Fig. 3 emphasizes two main points: (i) Current AMS techniques for ^{14}C analysis show excellent performance and enable the detection of low *in situ* ^{14}C concentrations with good precision. (ii) Reducing the uncertainties related to the blank correction can allow further lowering of the detection limit for *in situ* ^{14}C. This means not only reducing the blank level but more importantly minimizing the scatter in the blank data, thus, achieving the general objective of increasing the reproducibility of *in situ* ^{14}C analyses.

3.4. Reproducibility

To estimate the accuracy and precision of cosmogenic nuclide dating, a number of inter-laboratory comparison measurements of reference materials have been performed for different cosmogenic nuclides within the scope of the CRONUS-Earth project (Jull et al., 2015). For *in situ* ^{14}C, a total of 23 analyses of the CRONUS-A intercomparison material were performed at four different laboratories. A mean value of $(6.93 \pm 0.44) \cdot 10^5$ at g^{-1} qtz (1σ) with a coefficient of variation (CoV, % standard deviation) of 6.3% was found. This CoV is only slightly above the one for ^{26}Al analyses (4.9%) but clearly higher than the CoV for ^{10}Be (2.9%; Jull et al., 2015). Comparison of the CoV with the average analytical uncertainty reported from the laboratories show a pronounced overdispersion of the data set, i.e. reported analytical uncertainties for the single measurements were several times lower than the CoV of the entire dataset. This indicates that the reported analytical results do not account for all sources of variability that contribute to the uncertainties of the measured *in situ* ^{14}C concentrations and therefore reported uncertainties might systematically underestimate the actual uncertainties (Phillips et al., 2016a). However, the strong overdispersion is not unique for *in situ* ^{14}C data but was to a variable extent also observed for the other cosmogenic stable and radioactive nuclides, most pronounced for ^{36}Cl, ^{21}Ne, and ^{26}Al. Since the CoV values reported from the different laboratories for their individual datasets are also on the order of 5–6%, i.e. similar to the CoV of 6.3% for the combined data of all laboratories (Jull et al., 2015), overdispersion in the CRONUS-A *in situ* ^{14}C data most probably indicates an underestimation of the intra-laboratory variability. Inter-laboratory scatter seems to be of minor importance. This means that in many cases analytical uncertainties of *in*

situ ^{14}C concentrations might not sufficiently account for the full contribution of the external reproducibility to the total uncertainty. As pointed out by Hippe et al. (2014) and Lupker et al. (2015), researchers reporting *in situ* ^{14}C data should fully propagate not only AMS measurement errors and errors associated with the blank correction but also include an uncertainty related to intra-laboratory scatter.

It should be noted that the evaluation of *in situ* ^{14}C analytical reproducibility based on the data of the CRONUS-A reference material is representative for high-concentration samples only, for which AMS counting errors and blank contributions are comparatively low. Although low-concentration reference materials (CRONUS-N and CRONUS-R) were distributed, determining the *in situ* ^{14}C concentrations in these materials has proven challenging (Goehring et al., 2014; Fülöp et al., 2015b). The only results of CRONUS-N analyses reported so far have provided a mean *in situ* ^{14}C concentration of $(1.3 \pm 0.7) \cdot 10^4$ at g^{-1} ($n = 5, 1\sigma$) and a very low reproducibility of around 50% (Lupker et al., 2015). This excessive scatter can be mostly attributed to the dominant influence of the blank correction. In contrast, AMS counting errors for the CRONUS-N results alone are in the range of 3–5% emphasizing the excellent performance of current AMS systems in the analysis of very low *in situ* ^{14}C concentrations.

Clearly, further improvement of *in situ* ^{14}C analytical methods is needed to increase the overall reproducibility and achieve high accuracy and precision comparable to ^{10}Be measurements (Phillips et al., 2016b). One step towards more consistent intra-laboratory sample processing conditions and, thus, increased reproducibility could be achieved by automation of the *in situ* ^{14}C extraction and purification techniques. Recent measurements of the CRONUS-A sample (Jull et al., 2015) presented by Lifton et al. (2015) from an automated extraction system have given excellent reproducibility with a CoV of 0.6% ($n = 6$). The blank data of Lifton et al. (2015) suggest that improvement can also be achieved in the reproducibility of low-concentration measurements due to system automation. This should be verified by further data.

4. Paired *in situ* ^{14}C-^{10}Be analysis in glacial landscapes

Surface exposure dating using a single cosmogenic nuclide relies on two fundamental assumptions: (i) complete and uninterrupted surface exposure (with respect to the nuclide's half-life), and (ii) no nuclide inheritance (e.g., Gosse and Phillips, 2001; Ivy-Ochs et al., 2007; Akcar et al., 2011; Balco, 2011; Heyman et al., 2011). Assumption (i) requires that the dated rock surface has not been shielded from cosmic rays during the entire duration of exposure, thus, excluding surface cover by glacier readvance or partial surface shielding by seasonal snow, sediment cover etc. In the case of dating moraine boulders or erratics it also presumes that the boulders have not been turned or lost part of their surface by weathering, frost-cracking or other erosional processes. Any unaccounted for shielding or partial loss of the dated surface will lead to an underestimation of the exposure age. Assumption (ii) implies that the nuclide inventory in the dated surface was entirely accumulated during the recent episode of surface exposure. This condition is met if the rock surface has never been exposed to cosmic rays before or if any nuclides accumulated during a previous exposure event have been efficiently removed by glacial erosion or had sufficient time to decay. Since radioactive decay is minor to negligible for the "long-lived" ^{10}Be, ^{26}Al and ^{36}Cl nuclides on Late Quaternary to Holocene timescales, nuclide resetting depends on efficient glacial erosion. However, glacial erosion can be highly variable and depends on the erosion mechanisms, ice dynamics and the thermal conditions as the base of the ice (e.g., Hallet et al., 1996; Hildes et al., 2004). Under cold-based glaciers and polythermal ice sheets, the ice at the base remains (partially) frozen to the bedrock inhibiting glacier sliding and subglacial abrasion (Kleman, 1994; Kleman and Hättestrand, 1999; Kleman and Glasser, 2007). Thus, cosmogenic nuclides can accumulate in the rock surface over several exposure-burial periods, i.e. glacial-interglacial cycles, and build up nuclide inheritance which limits the ability to date the last deglaciation event (Bierman et al., 1999; Fabel et al., 2002; Briner et al., 2006, 2014; Harbor et al., 2006; Corbett et al., 2013). Glacially-transported boulders are often preferred over bedrock surfaces for exposure dating as boulders are more likely to fulfil the above conditions for simple exposure dating (Putkonen and Swanson, 2003; Heyman et al., 2011; Stroeven et al., 2011). However, in a compilation of global ^{10}Be exposure ages from glacial boulders Heyman et al. (2011) have shown that incomplete exposure due to surface shielding after boulder deposition is in fact an important process for creating geologic scatter in exposure ages. Several studies further found that erratics deposited during one glaciation can remain in position even after more than one subsequent advance and retreat of cold-based glacier ice (e.g., Stone et al., 2003; Sugden et al., 2005; Fogwill et al., 2014).

Resolving nuclide inheritance or interrupted surface exposure requires the analysis of two nuclides with different half-lives that will exhibit disequilibrium due to differential decay in a surface shielded by glacier ice. Until recently, the ^{10}Be-^{26}Al nuclide pair has been predominantly used for complex exposure dating, especially for studying glacier chronologies at high latitude sites and in the polar regions (e.g., Bierman et al., 1999; Fabel et al., 2002, 2006; Li et al., 2008; Glasser et al., 2012; Gjermundsen et al., 2015). Few studies also combined ^{10}Be with the stable nuclide ^{21}Ne (e.g., Ivy-Ochs et al., 2006; Di Nicola et al., 2007; Balco et al., 2014). However, because of their long half-lives the ^{10}Be-^{26}Al pair is only sensitive to changes in surface exposure on timescales of 100 ka to few Ma. This represents a major drawback for dating glacier fluctuations during the last glacial period and in particular the final major deglaciation event after the Last Glacial Maximum (LGM, ~20 ka). Detecting relatively recent complex exposure histories is therefore only possible with a nuclide of much shorter half-life as given by *in situ* cosmogenic ^{14}C. *In situ* ^{14}C can be applied for surface exposure dating over the past ca. 20–25 ka (~3–4 half-lives) before it reaches secular equilibrium (i.e. saturation). As such, it perfectly covers the post-LGM time range and can be ideally used to unravel complex surface exposure histories during the latest Pleistocene and Holocene.

4.1. Basic concept for dating complex glacier chronologies

Complex surface exposure dating typically combines *in situ* ^{14}C with ^{10}Be. Since all present extraction systems use quartz as target mineral for *in situ* ^{14}C extraction, sample processing for *in situ* ^{14}C and ^{10}Be (and ^{26}Al) can be performed on aliquots of the same purified quartz material. The use of the *in situ* ^{14}C-^{10}Be chronometer follows the general concept of (^{10}Be-^{26}Al) burial dating. It exploits the fact that nuclides with different half-lives will decay at different rates once a sample is buried and shielded from the cosmic-ray flux. The resulting change in the nuclide ratio will then provide a measure of the duration of burial. The development of the *in situ* ^{14}C-^{10}Be nuclide concentrations through a deglaciation-readvance-deglaciation cycle for a bedrock surface under the assumption of negligible glacial erosion by the readvancing glacier is illustrated in Fig. 4 (adapted from Zreda and Lifton, 2000):

(I) In the first stage of surface exposure both nuclides accumulate in the rock according to their individual production rates. The nuclide concentration ratio is defined by the production rate ratio, the ^{14}C half-life and the surface erosion rate. At t_1,

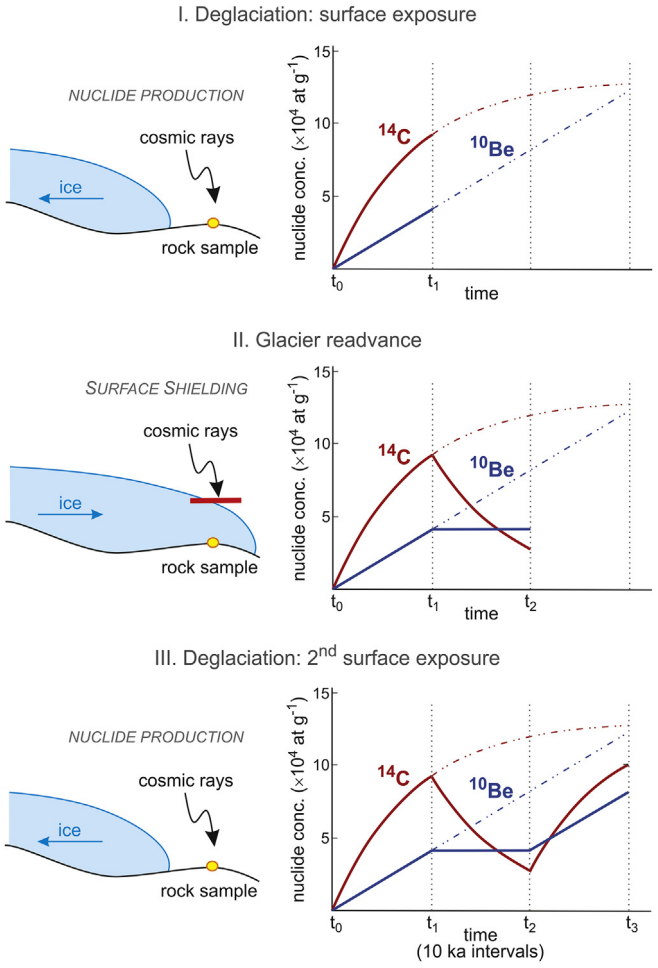

Fig. 4. Concept of complex surface exposure dating with combined *in situ* ^{14}C-^{10}Be analysis. A simple three-stage scenario of exposure-readvance-exposure is shown over an equal time interval of 10 ka for each phase. Shielding during glacier readvance is assumed to be complete; no erosion during exposure or by subglacial processes is included.

conditions for simple exposure dating are fulfilled and both nuclides will yield identical surface exposure ages.

(II) The second stage is characterized by glacier readvance and shielding of the bedrock from cosmic rays by thick ice. Thus, any further nuclide production ceases. During this stage, the *in situ* ^{14}C concentration rapidly decreases in consequence of the short ^{14}C half-life while the ^{10}Be concentration remains virtually unchanged. At t_2, i.e. immediately after re-exposure following the shielding event, the bedrock surface will show a ^{14}C/^{10}Be ratio clearly different from the production ratio. Measured nuclide concentrations will yield a mismatch in the apparent exposure ages with the *in situ* ^{14}C age being younger than the ^{10}Be age. The *in situ* ^{14}C and ^{10}Be concentrations at t_2 provide a unique solution of both the timing of initial deglaciation as well as the timing of glacier readvance. The ^{10}Be concentration records the time interval of surface exposure while the amount of ^{14}C lost by radioactive decay quantifies how long the rock surface has been buried under ice. In practical terms this means that the sampled surface must have been glacially covered until recently (at most until a few hundred years ago). Although such conditions might today be found in polar regions and present glacier forefields, many previously glaciated landscapes at mid to low latitudes have been ice free for several thousands to more than ten thousand years. Consequently, these surfaces have been re-exposed sufficiently long to experience further significant accumulation of cosmogenic nuclides. The result of such an exposure-burial-exposure history on the rock's nuclide inventory is illustrated in stage III.

(III) Stage III records additional nuclide production during the second phase of surface re-exposure. Similar to the situation at t_2, the ^{14}C/^{10}Be ratio in the bedrock surface sampled at t_3 will be in disequilibrium and the apparent *in situ* ^{14}C exposure age will be younger than the ^{10}Be age. However, the measured *in situ* ^{14}C-^{10}Be concentrations at t_3 do not provide a single solution for the timing of the individual deglaciation-readvance-deglaciation events. Reconstructing these more complex sequences requires independent age information or estimates that constrain the timing of either of the three stages. Such independent constraints can be derived by other dating methods (e.g. radiocarbon) or local to global climate archives.

4.2. Subglacial erosion

Paired *in situ* ^{14}C-^{10}Be analyses in previously glaciated surfaces can also provide a means for constraining subglacial erosion rates. Based on the amount of nuclide inheritance measured in formerly glaciated bedrock which is a function of bedrock removal by subglacial erosion, cosmogenic nuclides have been repeatedly used to constrain subglacial erosion depths (e.g., Briner and Swanson, 1998; Stroeven et al., 2002; Dühnforth et al., 2010; Young et al., 2016; Wirsig et al., 2017). However, a major condition is a well-constrained ice-cover and deglaciation history of the study area. This can be established with the help of *in situ* ^{14}C. The coupled *in situ* ^{14}C-^{10}Be approach follows the idea of ^{26}Al-^{10}Be isochron dating (Balco and Rovey, 2008; Balco et al., 2008a) and relies on a set of samples that have experienced the same exposure-burial history (Goehring et al., 2013). Assuming a simple exposure-burial scenario (equivalent to stage II of Fig. 4, see above), samples collected from a recently exposed proglacial bedrock area should have the same *in situ* ^{14}C-^{10}Be ratios due to their identical glacial history. The offset of the measured *in situ* ^{14}C-^{10}Be ratio from the production ratio is primarily controlled by the loss of ^{14}C through decay during burial under the readvancing glacier (Fig. 5A). In principle, the duration of exposure and burial can then be determined from the ^{14}C/^{10}Be ratio. However, in the case of subglacial erosion during burial, the ^{14}C/^{10}Be ratio will additionally be modified due to the changing ^{14}C/^{10}Be ratio in the subsurface (Fig. 5B) which is caused by the differences in muon contribution for *in situ* ^{14}C and ^{10}Be production (Fig. 1). Therefore, an additional constraint on either the timing of initial surface exposure or the timing of surface burial is needed. On the basis of the thus established surface chronology, depths of subglacial surface erosion can then be calculated for each individual sample using the differences in the measured *in situ* ^{14}C and ^{10}Be concentrations. Although a well-constrained glacier chronology is essential for the applicability of the *in situ* ^{14}C-^{10}Be pair to measure subglacial erosion rates, it offers the unique opportunity to investigate small-scale differences in subglacial abrasion, e.g. across a glacial trough or with respect to the bedrock geomorphology. The concept of using the relative differences between concentrations of two nuclides with a different production rate depth dependence to assess subglacial bedrock erosion has also been demonstrated with the ^{10}Be-^{36}Cl pair (Wirsig et al., 2017). In the light of the current retreat of many glaciers worldwide, the newly exposed glacier forefields provide the best study locations for this approach as they have not seen significant nuclide accumulation or subaerial surface erosion since re-exposure.

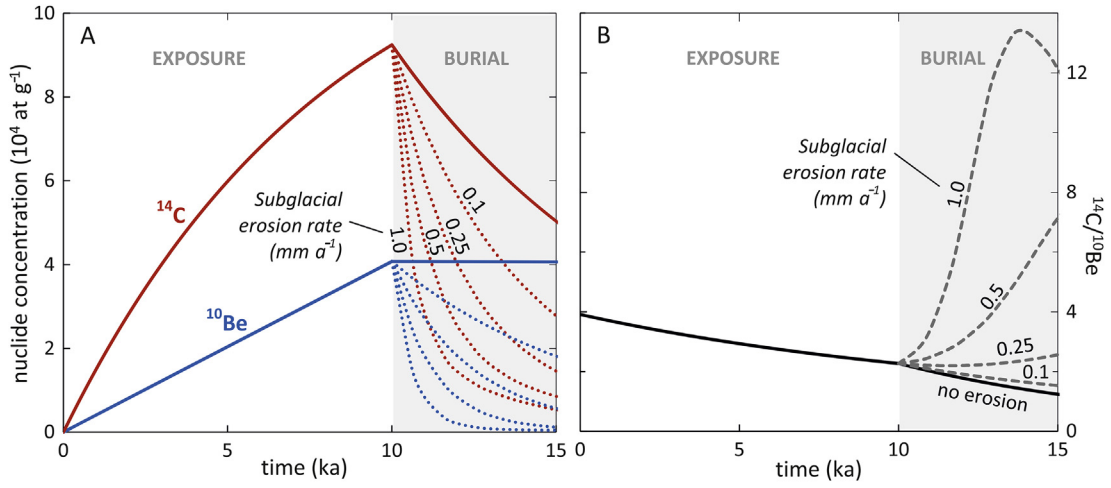

Fig. 5. The effect of subglacial erosion on the *in situ* ^{14}C and ^{10}Be nuclide concentrations for a simple exposure-burial scenario. A) Accumulation of both nuclides during 10 ka of exposure (at SLHL, no erosion) followed by nuclide loss during a 5 ka-period of surface burial due to glacier readvance. Solid lines during burial signify no subglacial erosion while dashed lines show increasing nuclide loss with increasing subglacial erosion rates. B) Development of the ^{14}C/^{10}Be ratio for the same exposure-burial sequence as in A). Again, the solid black line during burial represents the ^{14}C/^{10}Be ratio in the case of no subglacial erosion and grey dashed lines give the nuclide ratio for different subglacial erosion rates. Note that for high subglacial erosion rates the greater loss of ^{10}Be (due to low muon contribution at depth) by erosion creates an initial increase of the ^{14}C/^{10}Be ratio. After rapid removal of ^{10}Be, the fast ^{14}C decay leads to a subsequent decrease of the ^{14}C/^{10}Be ratio. Calculated for SLHL with a rock density of 2.65 g cm^{-3}. For production rates and calculation parameters see caption of Fig. 1.

4.3. Timeframe and sensitivity

The simplified three-stage exposure-burial-exposure scenario introduced above can be adapted to different geochronological contexts depending on the type of glacial landscape that is the subject of research. In mid-latitude glacial settings where highly erosive LGM ice is assumed to have largely reset the previously accumulated cosmogenic nuclide inventory, the beginning of stage I will in most cases coincide with the timing of initial deglaciation after the LGM. However, because of the large contribution of muonic production for *in situ* ^{14}C, subglacial erosion needs to erode rocks to a greater depth than necessary for resetting the ^{10}Be concentration (Fig. 1). For example, removal of 4 m of rock below a glacier will erase close to 99% of the ^{10}Be inventory but only 89% of the *in situ* ^{14}C concentration. To eliminate 95% of the *in situ* ^{14}C inventory the glacier needs to erode around 9 m of underlying bedrock. On the other hand, the rapid loss of ^{14}C due to decay contributes to the nuclide loss by subglacial erosion. After 10 ka of complete shielding, 95% of the *in situ* ^{14}C nuclides are removed with a total subglacial erosion of only 2.4 m (Fig. 6). Thus, re-zeroing of previously accumulated *in situ* ^{14}C during the LGM glaciation appears highly likely. In this scenario, stage II glacier readvance that causes intermittent surface shielding with ^{14}C decay under less erosive ice will then relate to post-LGM cold phases, particularly the Younger Dryas but also to Holocene climate fluctuations. The sensitivity of *in situ* ^{14}C to detect a period of readvance largely depends on the uncertainty in the obtained ^{14}C/^{10}Be ratio. Excluding production rate uncertainties, the uncertainty in the external reproducibility of *in situ* ^{14}C measurements is most important with a contribution of ~5–6% (Jull et al., 2015). Based on a 5% uncertainty on the measured *in situ* ^{14}C concentration, a burial time of at least 500 years should be detectable.

At higher latitudes, present-day ice caps and those expanding during the LGM frequently contained non-erosive basal ice. In these cases, the time window for the ^{14}C-^{10}Be chronometer is shifted back in time. For the three-stage model this means that nuclides accumulated during stage I can then represent pre-LGM surface exposure while stage II reflects surface shielding under readvancing LGM glaciers. Stage III consequently relates to the time of deglaciation after the end of the LGM. If surface shielding by thick LGM ice was sufficiently long to reduce the *in situ* ^{14}C inventory accumulated prior to the last glaciation to background levels (i.e. blank levels), the measured *in situ* ^{14}C concentration can provide a direct age estimate for deglaciation without the need for further

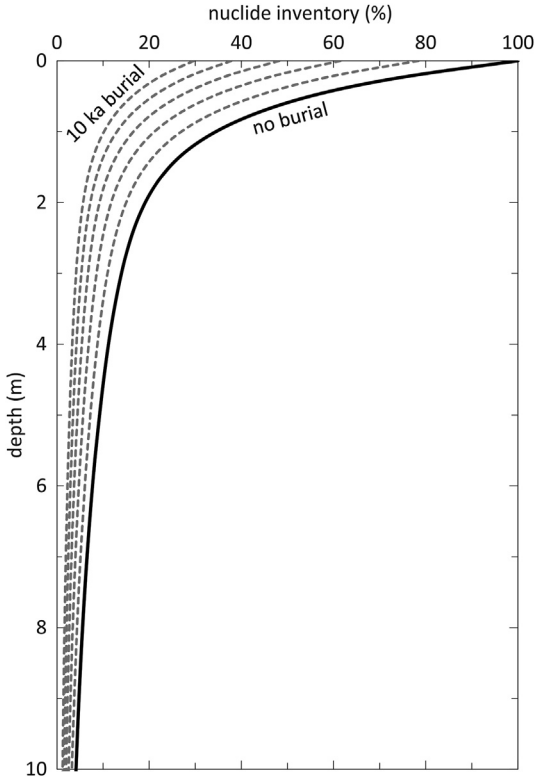

Fig. 6. Decrease of the *in situ* ^{14}C concentration with depth of subglacial erosion and nuclide decay due to surface burial by ice (complete shielding). Solid black line gives the relative concentration for no burial, dashed lines show decreasing concentrations with increasing burial time, calculated for 2 ka intervals. For production rates and calculation parameters see caption of Fig. 1.

independent age constraints. The possibility of complete resetting of the inherited signal under cold-based ice cover is one main benefit from the short ^{14}C half-life and a major motivation for its use in studies on glacier chronologies in the Arctic and Antarctic regions (cf. Miller et al., 2006; White et al., 2011; Briner et al., 2014; Fogwill et al., 2014; Bierman et al., 2015).

To assess the time required to reduce the *in situ* ^{14}C inventory in a glacially-shielded rock surface to near zero, two parameters have to be taken into account: the duration of surface cover and the thickness of the ice. As shown in Fig. 7A, a rock surface completely shielded from the cosmic-ray flux loses 95% of the previously accumulated ^{14}C nuclides after 25 ka (about five half-lives). After ~40 ka about 99% of the inherited ^{14}C nuclides will have decayed. In contrast, 98% and 96% of the inherited ^{10}Be and ^{26}Al nuclides are still present in the rock surface after 40 ka of complete shielding. However, due to the large contribution of muon-induced *in situ* ^{14}C production the total relative *in situ* ^{14}C production rate below a stack of ice of <100 m thickness is larger than the relative ^{10}Be production rate. This means that achieving complete shielding for *in situ* ^{14}C needs burial under a thicker amount of ice than needed to inhibit ^{10}Be production. Reducing the ^{10}Be production to 1% of its surface production rate is achieved by shielding with a comparatively thin glacier cover of about 13 m thickness (for a density of glacier ice of 0.92 g cm^{-3}). For the same shielding depth, *in situ* ^{14}C will maintain around 10% of its surface production rate. Reducing the *in situ* ^{14}C production rate in an ice-covered rock surface to the 1% level requires glacier ice of at least 70 m thickness (Fig. 7B). Thinner ice cover will allow for low but ongoing *in situ* ^{14}C production even during glaciation and result in apparently older *in situ* ^{14}C exposure ages.

4.4. Published examples of in situ ^{14}C-^{10}Be exposure dating of glacial landscapes

Three glacier systems have been in the focus of previous studies exploring combined *in situ* ^{14}C-^{10}Be dating for glacier chronology: (i) the Laurentide Ice Sheet (LIS), (ii) the Antarctic Ice Sheet and (iii) the Central Alpine glaciers (Fig. 8). Paired *in situ* ^{14}C-^{10}Be data of these studies are summarized in a two-nuclide diagram (Fig. 9) that allows an easy visualization of differences between both nuclides. Because the key point is the decrease of the *in situ* ^{14}C concentration, the diagram gives this value on the x-axis and the ^{10}Be/^{14}C ratio on the y-axis. As in the familiar ^{10}Be vs. ^{26}Al/^{10}Be two-nuclide diagram, given "burial lines" that indicate the time span required for surface burial to decrease the *in situ* ^{14}C concentrations to the measured values, apply to complete and uninterrupted shielding in a simple two-stage exposure-burial scenario (with burial until very recently). Thus, in many cases the burial duration that can be read from the diagram must be considered a minimum estimate.

4.4.1. Laurentide Ice Sheet

The extent and volume of the LIS, particularly during its last culmination, has been subject to extensive research and discussion (e.g., Dyke and Prest, 1987; Dyke et al., 2002; Marshall et al., 2002; Miller et al., 2002). Surface exposure dating with ^{10}Be and ^{26}Al of landscapes covered by the LIS has promoted great progress in reconstructing ice sheet history but has also shown the limitations of only using the ^{10}Be- ^{26}Al pair in areas of polythermal ice cover where the nuclide signal accumulated during one exposure event is not re-zeroed by subglacial erosion during a subsequent glaciation episode (summarized in Briner et al., 2006; Davis et al., 2006).

One of the first studies using combined *in situ* ^{14}C-^{10}Be-^{26}Al analysis investigated the efficiency of glacial erosion by the LIS and ice-sheet dynamics in the interior Canadian Arctic of Baffin Island (Miller et al., 2006). While the ^{26}Al/^{10}Be ratio was used to constrain

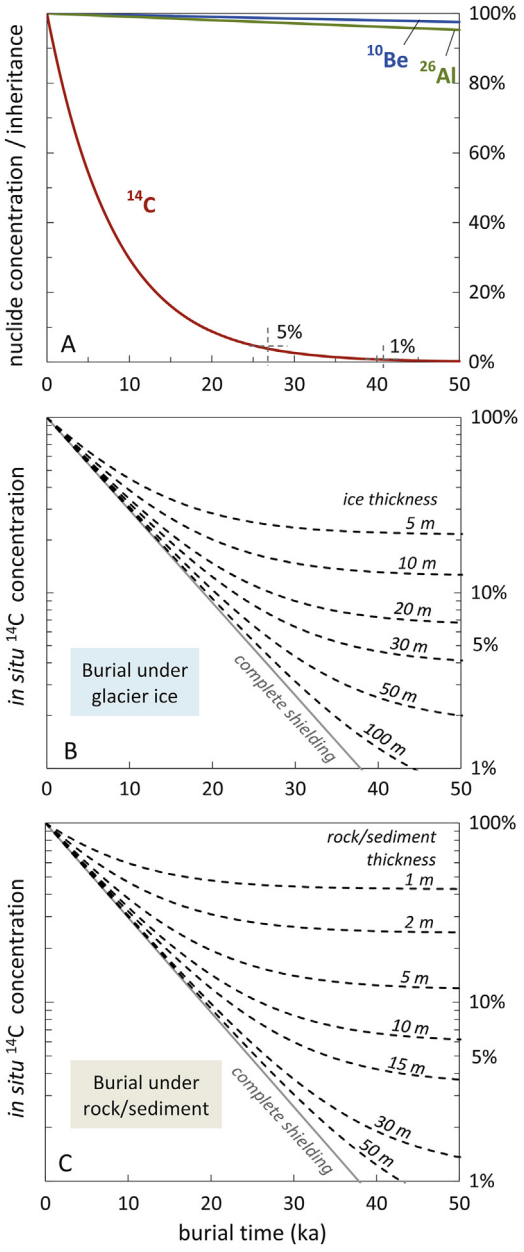

Fig. 7. Decrease of the cosmogenic nuclide concentrations during surface shielding. A) Comparison of the relative *in situ* ^{14}C, ^{10}Be and ^{26}Al concentrations during a burial interval of 0–50 ka assuming complete surface shielding from cosmic rays. B) Decrease of the relative *in situ* ^{14}C concentration over the same time interval due to shielding by glacier ice of different thickness; calculated for an ice density of $\rho = 0.92$ g cm^{-2}. C) Decrease of the relative *in situ* ^{14}C concentration in buried sediment over time. The sediment is shielded to a variable degree by overlaying rock or sediment of different thickness; calculated for a density of the overburden of $\rho = 2.0$ g cm^{-2}.

the long-term glacial history over at least the past 400 ka, the *in situ* ^{14}C exposure data determined the timing of late Pleistocene deglaciation and suggested a short episode (~1 ka) of surface cover by thin, cold-based ice caps during the late Holocene. Similar results with regard to the Holocene glacial evolution of the plateau ice caps across Baffin Island were reported by Anderson et al. (2008) who coupled measurements of *in situ* ^{14}C in quartz with radiocarbon dating of plant macrofossils emerging beneath the receding ice margins. Building on this study, Briner et al. (2014) combined published and new *in situ* ^{14}C measurements with ^{10}Be and ^{26}Al data to further unravel the complex deglaciation history of

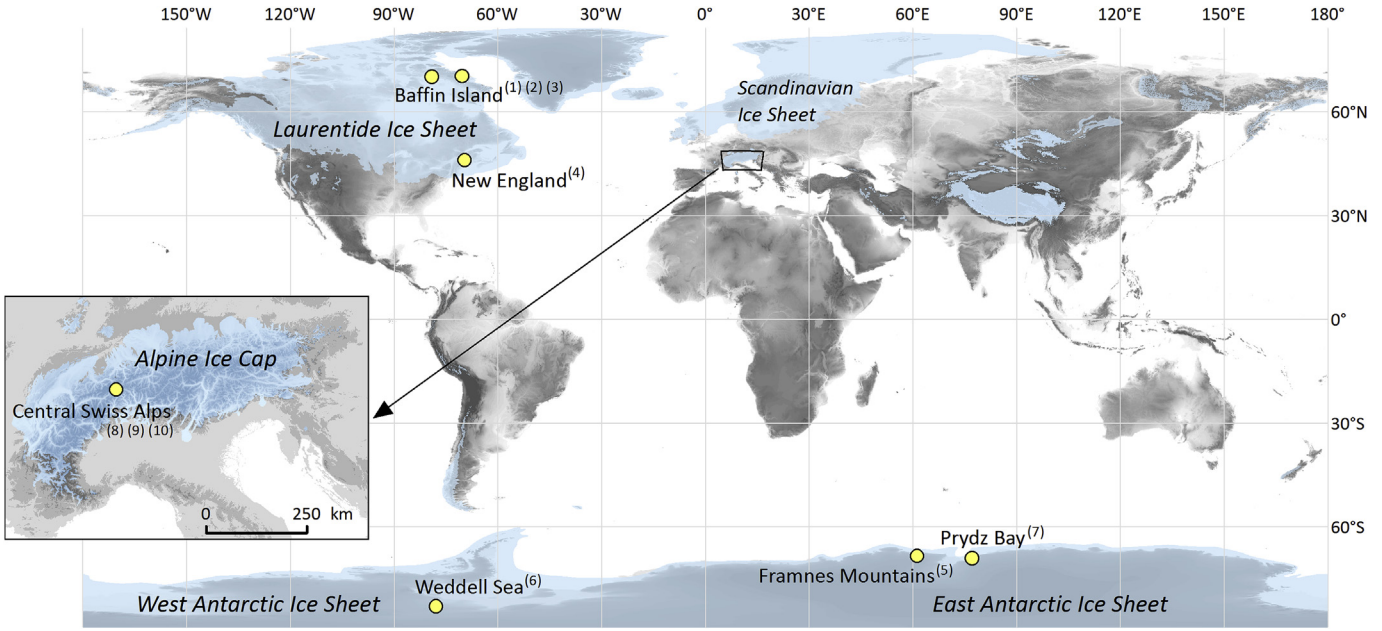

Fig. 8. Location map of the study sites for which paired *in situ* ^{14}C-^{10}Be data from glacial landscapes has been published. The map is also showing the extent of major ice sheets during the LGM (from Ehlers et al., 2011). (1) Miller et al. (2006), (2) Anderson et al. (2008), (3) Briner et al. (2014), (4) Bierman et al. (2015), (5) White et al. (2011), (6) Fogwill et al. (2014), (7) Berg et al. (2016), (8) Goehring et al. (2011), (9) Hippe et al. (2014), (10) Wirsig et al. (2016).

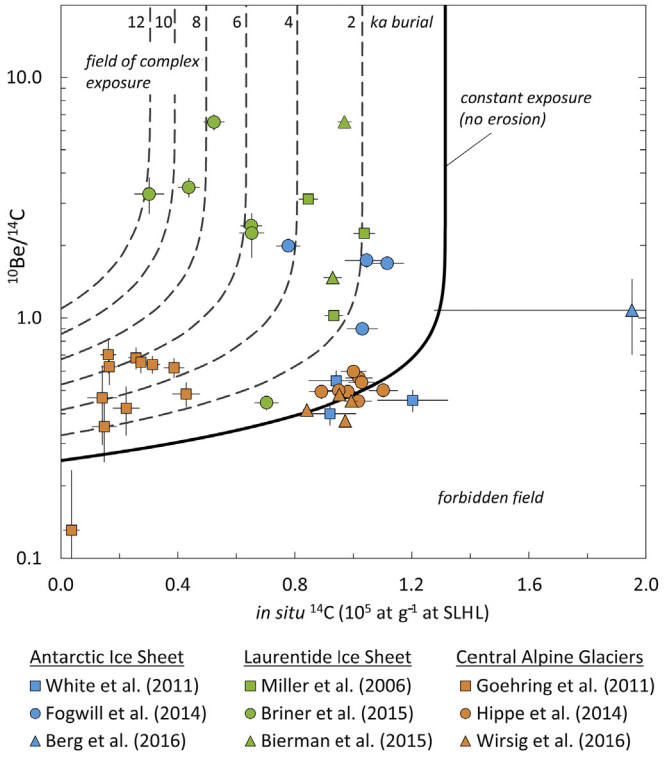

Fig. 9. Two-nuclide diagram of *in situ* ^{14}C vs. ^{10}Be/^{14}C summarizing hitherto published paired *in situ* ^{14}C-^{10}Be analyses from glacial settings. Published nuclide concentrations have been rescaled to SLHL using the MATLAB code from the online calculator (v. 2.3) of Balco et al. (2008b) with the scaling formula of Lal (1991)/Stone (2000) and modifications for paleomagnetic correction (Nishiizumi et al., 1989). Relative uncertainties on the nuclide concentrations as well as corrections for topographic shielding and sample thickness were applied as given in the original publications. The two-nuclide diagram was calculated using production rates and calculation parameters as given in the caption of Fig. 1.

Baffin Island (Fig. 10) and evaluate the long-term pattern of glacial erosion during the presence of the LIS. Based on the ^{10}Be-^{26}Al results, the authors propose a sharp boundary between sliding (erosive) and cold-based (non-erosive) conditions within the LIS that can be traced by the presence or absence of inheritance for these nuclides. However, since inheritance impeded accurate exposure dating with ^{10}Be and ^{26}Al only, the additional analyses of *in situ* ^{14}C proved invaluable to assess the timing of deglaciation and reconstruct episodes of Holocene neoglaciation. A study by Bierman et al. (2015) focussed on the highest summits of northern New England, USA, that have been previously occupied by the LIS. Significant inheritance detected for ^{10}Be and ^{26}Al was used to identify warm-based vs. cold-based conditions at the LGM glacier bed. With LGM glacial cover being sufficiently long to remove previously accumulated ^{14}C through radioactive decay, *in situ* ^{14}C concentrations recorded the timing of deglaciation as well as post-LGM partial shielding of the surfaces by till cover, snow or cold-based ice.

4.4.2. Antarctic Ice Sheet

Since organic material suitable for radiocarbon dating is largely absent in the Antarctic environment, cosmogenic-nuclide surface exposure dating has been crucial for reconstructing Antarctic Ice Sheet history (cf. Balco, 2011). However, more than 20 years of surface exposure dating in Antarctica has shown that many age data are affected by scatter due to different geologic processes, including surface burial by cold-based ice causing nuclide inheritance (Hein et al., 2014).

So far, few paired *in situ* ^{14}C-^{10}Be (and ^{26}Al) data from Antarctic samples have been published (excluding *in situ* ^{14}C data from saturated surfaces in Antarctica for production rate calibration; Borchers et al., 2016). In a first study, White et al. (2011) reported concordant ^{10}Be, ^{26}Al and *in situ* ^{14}C age data (within 2σ) obtained from three erratic boulders exposed from the East Antarctic Ice Sheet. As discussed by the authors, given the uncertainties on measurements and production rates of all three nuclides, it is not possible to unambiguously distinguish between a continuous

Fig. 10. Impressions from the different glacier systems studies with paired *in situ* ^{14}C-^{10}Be dating. Top: Weathered bedrock outcrop in front the present-day ice cap on Northern Baffin Island, Canadian Arctic (photo: courtesy of J. Briner). Considerable nuclide inheritance for ^{10}Be and ^{26}Al are evidence of cold-based glacier cover by the Laurentide Ice Sheet. Middle: Erratic boulder near the Weddell Sea embayment along the West Antarctic Ice Sheet (photo: courtesy of C. Fogwill). Nuclide inheritance in this and several other erratics from the area indicate the existence of cold-based ice during the LGM that left the boulders in position during glacier readvance. The timing of the complex exposure-readvance-exposure history could be determined by combined *in situ* ^{14}C-^{10}Be analysis and ice volume estimates from sea-level reconstruction. Bottom: Glacially-polished bedrock at the Central Alpine Gotthard Pass, Switzerland. Subglacial erosion that efficiently removed any pre-LGM nuclide inventory provided overall consistent ^{10}Be and *in situ* ^{14}C deglaciation ages.

surface exposure history and a complex exposure with only few ka of inheritance for ^{10}Be. White et al. (2011) further point out the particular difficulty to detect nuclide inheritance in the case of a comparatively long (recent) re-exposure which decreases the sensitivity of the ^{14}C/^{10}Be ratio. A study by Fogwill et al. (2014) investigated the response of the ice stream configuration in the Weddell Sea, West Antarctic Ice Sheet, to external forcing since the LGM. Chronological constraints on ice surface lowering were obtained by paired *in situ* ^{14}C-^{10}Be surface exposure dating (Fig. 10) in combination with global eustatic sea level data as an independent proxy for local ice volume. Samples for *in situ* ^{14}C measurements were chosen based on previously obtained ^{10}Be exposure ages that appeared to be “anomalously old”. Integrating the age data with high-resolution, whole-continent ice sheet modelling allowed identifying phases of post-LGM ice stream reorganization and Holocene changes in the mass balance of the investigated ice streams. Recently, Berg et al. (2016) reported a single *in situ* ^{14}C measurement performed in the context of a study on the evolution of the East Antarctic Ice Sheet during the last glacial cycle. In contradiction to previous estimates that have indicated early Holocene deglaciation, *in situ* ^{14}C analysis yielded a high nuclide concentration that is consistent with isotopic saturation, i.e. exposure $\geq$40 ka under very low subaerial erosion rates.

4.4.3. Central Alpine glaciers

In contrast to the research presented from polar regions where the issue of nuclide inheritance frequently occurs, LGM ice cover in the mid-latitude Alpine environment is often assumed to have been highly erosive (e.g., Nesje et al., 1992; Hallet et al., 1996; Riihimaki et al., 2005; Wirsig et al., 2017), which is also evidenced by the deeply carved Alpine valleys. With the cosmogenic nuclide clock being completely re-zeroed before surface exposure from the disappearing LGM ice, apparently “too old” ^{10}Be or ^{26}Al exposure ages are much less common than at high-latitudes (Kelly et al., 2006; Ivy-Ochs et al., 2007). However, in the European Alps glacier readvances during colder periods of the Lateglacial and Holocene are known but yet often remain poorly dated (e.g., Ivy-Ochs et al., 2007, 2009). Constraining these intervals of short-term glacier advances is an important issue in the reconstruction of post-LGM Alpine landscape evolution and provides vital information on the sensitivity of small high-Alpine mountain glacier systems to climate fluctuations.

Investigating fluctuations of the Rhone Glacier (Switzerland) in response to Holocene climate variations, Goehring et al. (2011) used paired *in situ* ^{14}C-^{10}Be analyses from recently exposed proglacial bedrock to quantify glacier growth or withdrawal compared to its present extent. Since the obtained ^{14}C/^{10}Be ratios were in agreement (within 2σ) with a mean calculated ^{14}C/^{10}Be ratio, the authors propose the same exposure-burial history for all samples and smaller extent of the Rhone glacier during most of the Holocene. Goehring et al. (2011) further presented the first approach using the ^{14}C/^{10}Be ratio to determine subglacial abrasion rates and their variability in relation to the position below the glacier tongue. Goehring et al. (2013) later applied a Bayesian isochron approach incorporating geologic constraints, e.g. glacial erosion, to recalculate their data from the Rhone glacier and obtain a better precision on the burial and exposure ages. This approach was re-evaluated by Beel et al. (2015) who published a sensitivity analysis of the *in situ* ^{14}C-^{10}Be isochron method using the data of Goehring et al. (2011). Just 15 km east of the Rhone glacier in the area of the Central Swiss Gotthard Pass (Fig. 10), Hippe et al. (2014) used paired *in situ* ^{14}C-^{10}Be exposure dating for reconstructing local deglaciation and the reorganization of the ice flow pattern during progressive downwasting of the Lateglacial ice surface. The obtained ^{14}C/^{10}Be ratios further allowed estimations on the thickness of seasonal snow cover that caused partial shielding of the otherwise entirely ice-free surfaces throughout the Holocene. A different approach to the question of subglacial erosion was presented by Wirsig et al. (2016) who applied combined *in situ* ^{14}C, ^{10}Be and ^{36}Cl analysis to study the Holocene evolution of the Grueben glacier (Central Switzerland). The authors made use of the fast ^{14}C decay to determine Holocene burial episodes and additionally aimed to exploit the sensitivity of ^{36}Cl to surface erosion to assess subglacial erosion

depths. Comparable to the differences in depth dependence between *in situ* ^{14}C and ^{10}Be caused by varying muon contribution (Fig. 1), production of ^{36}Cl at depth has distinct characteristics due to specific thermal neutron capture processes (Phillips et al., 2001). The three-nuclide method has the advantage that glacier chronology and subglacial erosion are determined independently so that robust results can be obtained without the need for additional external constraints on the timing of exposure and burial (for a recently re-exposed surface).

5. Beyond glacial landscapes: applications of combined *in situ* ^{14}C-^{10}Be analysis in sedimentary deposits, eroding surfaces and along fault scarps

Unravelling complex surface exposure histories in glacially modified landscapes has been a key target for combined *in situ* ^{14}C-^{10}Be dating. Nevertheless, the short half-life of *in situ* ^{14}C introduces various applications in sedimentary systems to quantify the processes in Earth surface development and landscape change. In principle, coupled *in situ* ^{14}C-^{10}Be analysis can follow the path of the ^{26}Al-^{10}Be pair but covering a shorter timescale (Holocene to latest Pleistocene). However, the interpretation of the *in situ* ^{14}C signal in sedimentary systems is less straightforward compared to the long-lived nuclides, particularly with regard to the integration of landscape-wide signals. According to the general concept, the cosmogenic nuclide inventory in an eroding surface depends on the rate of surface erosion while the loss of nuclides by radioactive decay is negligible. If erosion is very slow, however, the integration timescale (the time required to erode the depth of one absorption length of cosmic rays in the subsurface; $t = \Lambda/\varepsilon \cdot \rho$) can exceed the nuclide's half-life. In that case, radionuclides accumulated at or near the surface will decay before being eroded which reduces the nuclide concentration below the actual erosion-controlled steady-state level. For the long-lived ^{10}Be and ^{26}Al nuclides, erosion rates in most natural settings greatly outrun their very slow rates of radioactive decay. Due to its fast decay, however, this does not generally apply to *in situ* ^{14}C. Consequently, the *in situ* ^{14}C concentration measured in river sediments collected at a basin outlet might not represent an integrated basin-wide erosion signal in slowly eroding landscapes or landscapes with highly variable local erosion rates. This also implies a deviation of the ^{14}C-^{10}Be ratio from the erosion-controlled steady-state ratio. Moreover, in slowly eroding surfaces soil mixing processes can additionally decrease the *in situ* ^{14}C concentration and further reduce the ^{14}C-^{10}Be ratio. Another important aspect is the sensitivity of the ^{14}C-^{10}Be ratio to recent changes in the surface erosion rates or events of mass removal from the surface which can perturb the *in situ* ^{14}C-^{10}Be signal. The crucial point is to recognize the different processes that can influence the *in situ* ^{14}C concentration and the ^{14}C-^{10}Be ratio, respectively, in eroding surfaces and to take these factors into account when interpreting *in situ* ^{14}C data from sediment or soil samples. Although this might be considered as a hindrance in the use of *in situ* ^{14}C in sedimentary systems, it also opens up new opportunities to unravel and quantify variations in surface erosion rates or soil removal as well as soil mixing processes. Below, an overview on some possible applications is given. Not all of them have already been tested in a natural setting underlining that the true potential of the *in situ* ^{14}C-^{10}Be nuclide pair in quantitative geomorphology is not fully explored.

5.1. Dating young sediments: burial, isochron-burial and depth-profile dating

As shown for glacier shielding, burial dating of a bedrock surface or sediment package can be accomplished with *in situ* ^{14}C-^{10}Be over a 10^2–10^4 year timescale (Fig. 7A). In the footsteps of simple ^{26}Al-^{10}Be burial dating (e.g., Granger and Muzikar, 2001; Granger, 2006, 2014), the *in situ* ^{14}C-^{10}Be pair can, for example, be applied for dating cave sediments younger than ~25 ka. A major assumption for any dating of sedimentary deposits is that at the time of deposition the sediment has been in isotopic steady-state, meaning that the ^{14}C-^{10}Be ratio has not been modified by any of the processes discussed above. It is further important to note that owing to the large muon contribution to the *in situ* ^{14}C production, near-complete shielding of sediments washed into a cave requires a comparatively large overburden of ~50 m thickness (for a density of 2.0 g cm^{-3}, Fig. 7C). As such, the simple burial dating approach with *in situ* ^{14}C-^{10}Be is limited to deeply buried sediments for which post-burial production can be excluded. If, however, some amount of nuclide production during burial is likely, an accurate knowledge of the burial depth, the density of the overlying rock or sediment, the surface erosion rate, and the production rate depth profile is needed to accurately determine the post-burial production component (e.g., Granger, 2014). In this context, the muonic *in situ* ^{14}C production becomes particularly important.

For the ^{26}Al-^{10}Be pair, the method of isochron-burial dating has been developed, which allows disregarding post-burial production (Balco and Rovey, 2008; Erlanger et al., 2012; Balco et al., 2013). Isochron-burial dating is performed on a set of samples taken from within the same stratigraphic horizon which are assumed to have experienced the same post-burial history but have a variable inheritance signal. Consequently, the ^{26}Al vs. ^{10}Be concentrations of all samples will plot on a straight line whose slope denotes the burial age (Balco and Rovey, 2008; Erlanger et al., 2012; Granger, 2014). While this approach has introduced great advantages for ^{26}Al-^{10}Be burial dating (e.g., Granger et al., 2015; Matmon et al., 2015; Zhao et al., 2016, 2017), it will not be easily applicable for *in situ* ^{14}C-^{10}Be burial dating because the *in situ* ^{14}C vs.^{10}Be concentrations for samples of widely different inheritance will mostly not fall on a straight line. In consequence of the short half-life, the *in situ* ^{14}C concentrations in long-exposed erosional surfaces, i.e. in slowly eroding landscapes, approach steady-state and become less sensitive to resolve a variability in the inheritance signal. Fig. 11 illustrates the temporal development of the *in situ* ^{14}C vs.^{10}Be concentration for buried sediment starting from erosion-controlled steady-state conditions (solid black line). It is shown that for high inherited *in situ* ^{14}C concentrations (>10^5 at g^{-1}) the slopes of the lines denoting simple burial (grey dashed) and those including post-burial production (blue solid) will not be distinguishable, thus, preventing an accurate burial age determination. The chances to successfully apply *in situ* ^{14}C-^{10}Be isochron-burial dating seem to be better for lower inheritance concentrations and higher post-burial production (Fig. 11), e.g. in fast eroding landscapes and for shallow sediment burial. However, measuring such low nuclide concentrations usually also imply larger measurement uncertainties, often above 5% (Fig. 3).

Depth profile dating is another method commonly applied to determine the deposition age of a sedimentary deposit (e.g., Matmon et al., 2006; Hidy et al., 2010; Ciner et al., 2015). The approach is based on the assumption that a sediment section has been deposited during a single event and, thus, that a uniform average nuclide inheritance is present throughout the section profile (Anderson et al., 1996; Repka et al., 1997). Using the predictable post-depositional cosmogenic nuclide production at each depth, which will follow a roughly exponentially decreasing curve from the surface downwards, the inherited concentration, the time of deposition and the surface erosion rate at the top of the deposit can be modelled (Repka et al., 1997; Granger and Smith, 2000; Braucher et al., 2009; Hidy et al., 2010). Due to its fast decay, the development of the *in situ* ^{14}C concentration within a depth profile

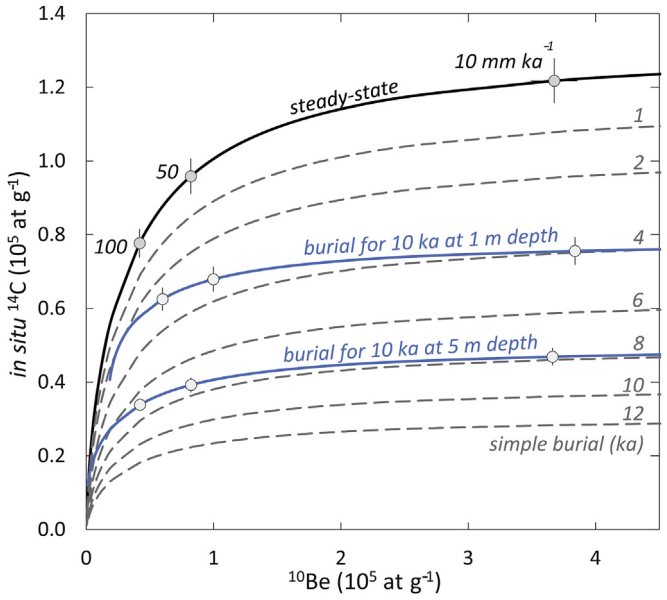

Fig. 11. ^{10}Be vs. *in situ* ^{14}C concentration in buried sediment, e.g. in a fluvial terrace. The sediment is assumed to leave the source area in isotopic steady-state controlled by the local surface erosion rate. As an example, three samples are shown here with concentrations equal to surface erosion rates of 10, 50 and 100 mm ka^{-1} (grey circles given with an assumed 5% analytical uncertainty). Grey dashed lines show the decrease of the *in situ* ^{14}C concentration from steady-state for the case of simple burial (i.e. complete shielding). Blue solid lines illustrate incomplete shielding with post-burial production, here calculated for continuous nuclide production during the entire burial episode of 10 ka for samples buried at 1 m and 5 m depth, respectively. The main observation is that the slope for the lines of simple burial and those including post-burial production are nearly identical, particularly for inherited *in situ* ^{14}C concentrations >10^5 at g^{-1}. Consequently, ages determined from the apparent loss of *in situ* ^{14}C compared to steady-state, will always be minimum ages only. Calculated for SLHL with a density of 2.0 g cm^{-3}; for production rates and calculation parameters see caption of Fig. 1.

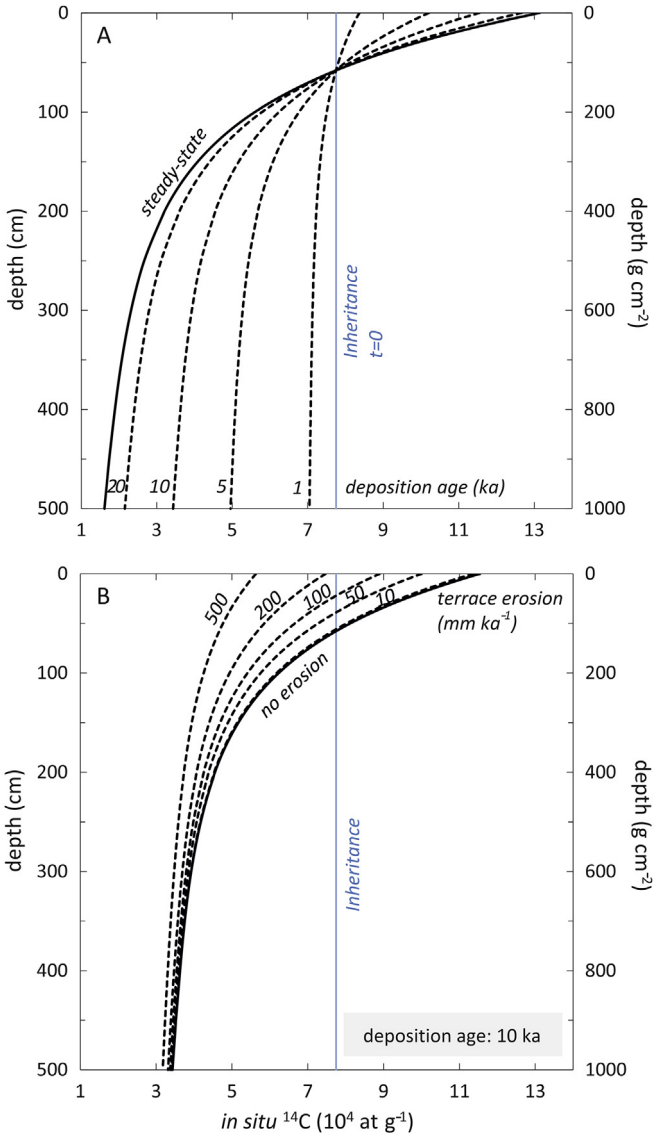

Fig. 12. *In situ* ^{14}C depth profiles in a sedimentary deposit, e.g. a fluvial terrace. Very fast deposition is assumed for the entire sediment stack allowing for a uniform inheritance concentration (blue vertical lines). (A) With increasing deposition age the *in situ* ^{14}C concentration at depth rapidly decreases towards steady-state at ~25 ka (no surface erosion). (B) The *in situ* ^{14}C concentration at the surface is sensitive to the rates of terrace erosion which can be resolved for rates > 25 mm ka^{-1} (when assuming a 5% analytical uncertainty on the *in situ* ^{14}C data). For both diagrams an inherited concentration of 7.75 × 10^4 ^{14}C at g^{-1}, equivalent to sediment provenance from a source area eroded with about 100 mm ka^{-1}, has been used. Calculated for SLHL with a density of 2.0 g cm^{-3}; for production rates and calculation parameters see caption of Fig. 1.

differs significantly from the one for ^{10}Be. Most notably is the rapid decrease of the *in situ* ^{14}C concentration at depth with a strong deviation from the inheritance concentration with increasing age of sediment deposition (Fig. 12A). With the rapid approach to steady-state, dating of sedimentary deposits with *in situ* ^{14}C depth profiles is limited to ~25 ka. Similar to ^{10}Be, the *in situ* ^{14}C concentration at the surface is rather sensitive to the erosion rate of the sediment deposit although small erosion rates below ~25 mm ka^{-1} are negligible (Fig. 12B). For very accurate dating of young deposits, the combination of *in situ* ^{14}C with ^{10}Be depth profiles could provide a valuable approach. Since the ^{10}Be concentration at depth will preserve the inherited signal over short time-scales, the ^{14}C-^{10}Be ratio at depth will be very sensitive to variations in deposition age, even for depths of only few meters.

5.2. Quantifying sediment storage and transfer times

An exciting application that has only been little explored is the use of the *in situ* ^{14}C-^{10}Be chronometer to investigate sediment routing and periods of sediment storage within fluvial systems. Analysing *in situ* ^{14}C-^{10}Be in river sediment, provides a method to directly determine episodes of sediment storage during transfer from source to sink and to assess sediment residence times within a fluvial basin (e.g., Brown et al., 1995; Wittmann and von Blanckenburg, 2009; Hippe et al., 2012). The concept of dating sediment storage times is in principle very similar to the idea of dating complex deglaciation histories (Fig. 4). Again, the underlying assumption is that the eroded sediment has left the source area in isotopic steady-state or that the original ^{14}C-^{10}Be ratio is known or can be reasonably assumed, e.g. from measurements of *in situ* ^{14}C-^{10}Be in source area surface samples. Fig. 13 illustrates the main steps: (i) Surface denudation in the bedrock source area releases sediment with steady-state *in situ* ^{14}C and ^{10}Be concentrations that are defined by the local erosion rates. (ii) Sediment transport is interrupted by sediment storage, e.g. through deposition in fluvial terraces. During storage (assuming complete shielding in this example), the *in situ* ^{14}C concentration will decrease while the ^{10}Be concentration hardly changes. (iii) After remobilization of the sediment it is transported quickly downstream where it is sampled from the active stream. The measured concentrations within the river sediment will then yield a deviation of the ^{14}C/^{10}Be ratio from

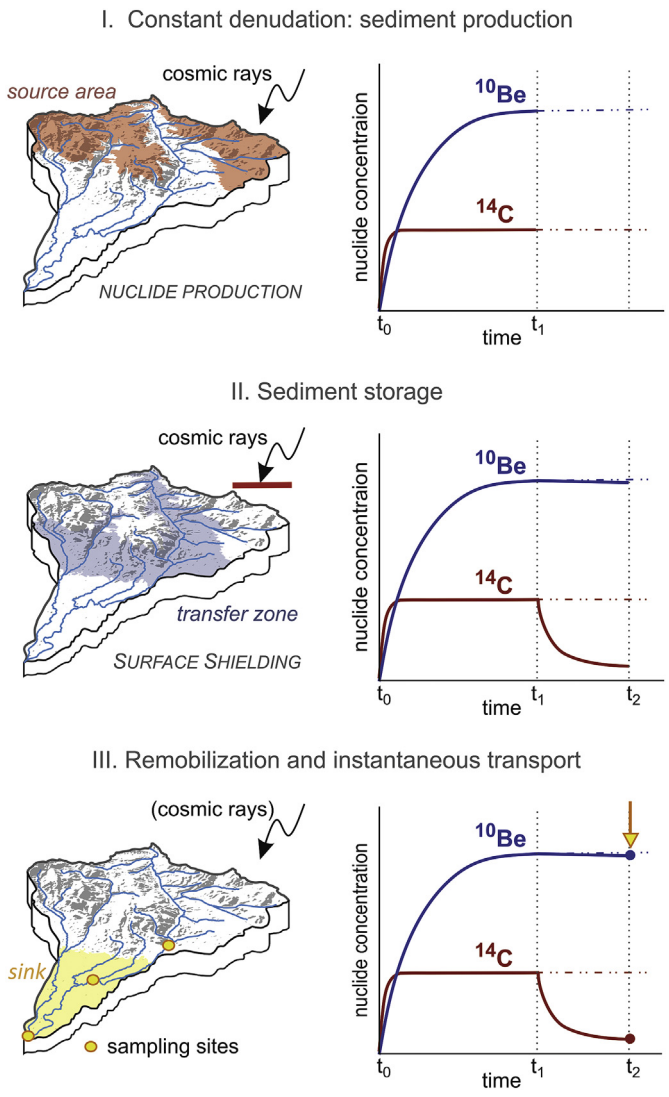

Fig. 13. Simplified view on the path of sediment through a catchment illustrating the concept of sediment storage time quantification with combined *in situ* ^{14}C-^{10}Be analysis. Both nuclides are assumed to be in erosion-controlled steady-state when leaving the source area and sediment storage is associated with deep burial, i.e. complete shielding of the sediment from the cosmic-ray flux. Although here only one storage event and quick transport after remobilization is assumed, naturally the *in situ* ^{14}C concentration measured in fluvial sediment could also record an integrated decay signal of repeated storage episodes. Note that the y-axes on the nuclide diagrams are not to scale. The t_1-t_2 time window equals a time range of about 20 ka.

the initial steady-state production ratio. Since the actual time of active sediment transport is assumed to be negligible, the *in situ* ^{14}C concentration will record the integrated duration of sediment storage whereas the ^{10}Be concentration will preserve the signal of the long-term sediment production/surface erosion rate within the source area. Sampling of sub-basins along the main channel or within tributaries allows to pinpoint in detail the individual storage sites and the time the sediment spends at each site on its pathway through the basin. In the simplest but rather rare case, sediment storage encompasses complete shielding of the sediment from the cosmic-ray flux. In most other cases, however, a post-burial production component has to be included into the calculations to obtain accurate storage durations. Field observations on the depth of river incision into sedimentary deposits can provide independent constraints on the average storage depth within the study area. Depending on the *in situ* ^{14}C measurement uncertainties, storage times of several 10^3–10^4 years should be well-detectable.

The great potential of the *in situ* ^{14}C-^{10}Be pair for studying surface fluxes and residence times in sedimentary fluvial systems has been theoretically modelled in some detail for a variety of large river basins with different floodplain residence times (Wittmann and von Blanckenburg, 2009; Lauer and Willenbring, 2010). However, applications to natural settings have been few so far. In a steep Alpine fluvial catchment (Central Switzerland), Kober et al. (2012) reported a few thousand years of sediment storage for colluvium and glacial sediments prior to their remobilization by debris-flows events. In a largely different setting on the low-relief Altiplano plateau (Bolivia), Hippe et al. (2012) used combined *in situ* ^{14}C-^{10}Be-^{26}Al analyses to determine sediment production rates and sediment transfer times in fluvial catchments along the Eastern Altiplano edge. Concordant ^{10}Be-^{26}Al data were interpreted as reflecting low, long-term steady-state surface erosion rates (10^4–10^5 year timescale) while comparatively low *in situ* ^{14}C concentrations seemed to indicate a considerable interruption of sediment transport by storage at shallow depths. Finally, in a recent study by Kim et al. (2016) overall concordant *in situ* ^{14}C-^{10}Be data from river sediments at the former rift-flank margin of the Korean Peninsula allowed confirming the absence of significant sediment storage and agree with the near steady-state conditions that have been suggested from local geomorphology.

5.3. Detecting landscape transience and rapid surface erosion events

Another, yet unexplored application is to couple *in situ* ^{14}C analyses to ^{10}Be measured in hillslope sediments to investigate transience in actively eroding landscapes. The high sensitivity of *in situ* ^{14}C to recent, short-term changes in surface erosion offers the opportunity to detect erosion transience and infer the timing and magnitude of erosion rate change or the thickness of mass removed during an instantaneous mass erosion event (Hippe et al., 2013a; Mudd, 2016). This is based on the idea that any change in the erosion rate will be recorded by the nuclide concentrations with a significant lag time that depends on the nuclide's half-life. Thus, the much faster adjustment of the *in situ* ^{14}C concentration to the new erosion signal in comparison to ^{10}Be creates an offset between the apparent *in situ* ^{14}C and ^{10}Be erosion rates and a deviation of the ^{14}C-^{10}Be ratio (cf. Mudd, 2016). As illustrated in the simple scenario of a rapid step change in erosion rates (Fig. 14), the highest offset in the ratio between apparent *in situ* ^{14}C and ^{10}Be erosion rates (^{14}C ε_{app}/^{10}Be ε_{app}), i.e. the highest sensitivity of the *in situ* ^{14}C-^{10}Be pair, is given for events younger ~25 ka and for rather low surface erosion rates in the range of few mm ka^{-1}. For high surface erosion rates in the range of several 100–1000 mm ka^{-1} the deviation of the ^{14}C ε_{app}/^{10}Be ε_{app} ratio gets comparatively small and will be difficult to detect (Fig. 14A). However, the sensitivity to detect a change in surface erosion rates in the past increases with the magnitude of the change (Fig. 14B). Fig. 14C further shows the case of an increase in erosion rates that is accompanied by an instantaneous loss of mass from the surface, e.g. by soil stripping. Although the nuclide ratios are not unique in all cases, *in situ* ^{14}C-^{10}Be pair allows modelling the timing of erosion rate acceleration or deceleration as well as the initial and changed erosion rates or the amount of material that has been removed from the surface. A huge benefit is the fact that the erosion event or change can be detected at the site where it happened. This is an advantage to the common assessment of variations in surface erosion from the sedimentary records of the downstream deposition areas which requires an effective source-to-sink coupling and can be biased by long sediment transit times (e.g., Phillips, 2003; Jerolmack and Paola, 2010).

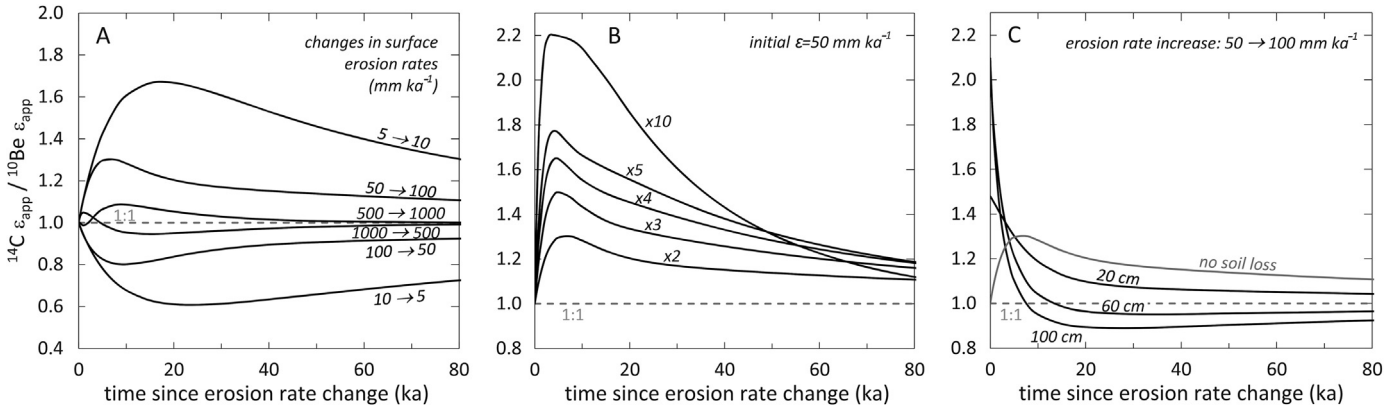

Fig. 14. Impact of a rapid change in surface erosion rates on the ratio between apparent *in situ* ^{14}C and ^{10}Be erosion rates ($^{14}C\ \varepsilon_{app}/^{10}Be\ \varepsilon_{app}$) for the cases of: (A) a doubling of erosion rates in fast vs. slowly eroding landscapes, (B) various magnitudes of erosion rate increase (starting from an initial rate of 50 mm ka^{-1}), and (C) doubling of erosion rates (50–100 mm ka^{-1}) accompanied by an instantaneous removal of soil of various depths from the surface. Calculated for a rock density of 2.65 g cm^{-3}; for production rates and calculation parameters see caption of Fig. 1.

Following a slightly different approach, Fülöp et al. (2015a) proposed combined *in situ* ^{14}C and ^{10}Be analyses in soil depth profiles to determine rates of surface erosion or date events of rapid soil loss. It follows an idea presented in a study by Lal et al. (1996) who measured *in situ* ^{14}C and ^{10}Be in a quartz vein in a soil profile to model past variations in soil erosion rates. This approach compares a measured depth profile with a theoretical depth profile (of known age or in steady-state) and exploits the fast adjustment of the *in situ* ^{14}C concentration in a depth profile truncated by a surface erosion event to the theoretical zero-erosion profile. In their investigation of Younger Dryas moraines in Scotland, Fülöp et al. (2015a) analysed two depth profiles through the moraine deposits and modelled the timing of a Holocene soil erosion event as well as the amount of soil removal based on a known moraine deposition age.

5.4. Influence of soil mixing on the in situ ^{14}C surface concentration

On soil-mantled hillslopes the occurrence of soil mixing that causes vertical particle transport by bioturbation and/or cryoturbation processes might detectably affect the nuclide concentration (Brown et al., 1995; Granger and Riebe, 2007; Schaller et al., 2009; Hippe et al., 2012). From a cosmogenic nuclide perspective, quartz grains with low nuclide concentrations are brought from depth towards the surface, while quartz grains with high nuclide concentrations are transported downwards. In the idealized case of complete mixing the nuclide concentration should be equal throughout the entire mixed soil layer (Fig. 15). However, the actual concentration strongly depends on the soil/surface erosion rate and the half-life of the cosmogenic nuclide. In slowly eroding surfaces (ε lower than ~100 mm ka^{-1}), the *in situ* ^{14}C concentration within the well-mixed soil is essentially controlled by radioactive decay and the depth of the mixed soil layer (Fig. 15B). This holds the potential to quantify the depths of soil mixing processes and reveal changes between past and modern mixing depths, e.g., in relation to climate change or human land use. Although model calculations on the theoretical development of the *in situ* ^{14}C concentration at the surface for increasing soil mixing depths have been presented (Fig. 6 in Hippe et al., 2012) field studies to further explore this concept are lacking so far.

5.5. Dating fault scarps

Surface exposure dating of vertical fault scarps with cosmogenic nuclides is dominated by applications of ^{36}Cl dating in limestones (e.g., Zreda and Noller, 1998; Mitchell et al., 2001; Benedetti et al., 2002; Schlagenhauf et al., 2011; Akcar et al., 2012). Few studies have also applied ^{10}Be (and ^{26}Al) in silicates for direct dating of fault planes and the determination of fault slip rates (e.g., Hippolyte et al., 2006; Kong et al., 2010). The use of *in situ* ^{14}C for fault scarp dating has been uniquely examined by Harrington et al. (2000) in a study on neotectonic activity in the Yucca Mountains of Nevada (USA). The authors presented *in situ* ^{14}C data measured in whole rock samples of welded tuff exposed along several fault scarps and found Holocene exposure ages as well as many saturated

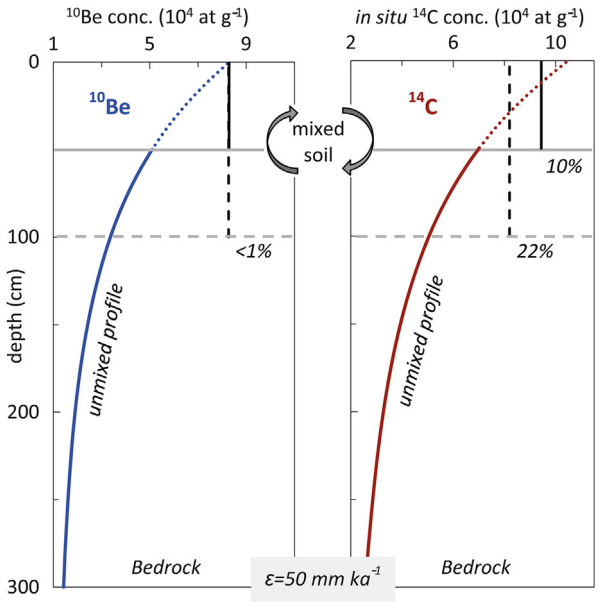

Fig. 15. The effect of mixing processes in soil-mantled, slowly eroding surfaces on the ^{10}Be and *in situ* ^{14}C concentrations at the surface and within the mixed layer. Blue and red solid lines illustrate the exponential depth dependence of both nuclides in the absence of soil mixing, given for a constant surface denudation rate of 50 mm ka^{-1}. Black vertical lines give the nuclide concentrations in a well-mixed soil layer for mixing depths of 50 cm (solid line) and 100 cm (dashed line). While the ^{10}Be concentration records the erosion-controlled surface concentration throughout the mixed layer, the "mixed" *in situ* ^{14}C concentration is considerably lower compared to the non-mixed surface concentration and decreases further with increasing mixing depth (as given by the deviation from the unmixed surface concentration in %). Calculated for an averaged substrate density of 2.0 g cm^{-3} using the modified equations of Brown et al. (1995) and Schaller et al. (2009) following the descriptions given in Hippe et al. (2012); for production rates and calculation parameters see caption of Fig. 1.

surfaces (exposure >20 ka). As illustrated in the theoretical distribution of *in situ* ^{14}C within a stepwise exposed fault plane (Fig. 16), the fast approach of *in situ* ^{14}C to the saturation concentration makes this application most useful on Holocene timescales. Since the analysis of whole rock samples has been given up for *in situ* ^{14}C, its use is now limited to quartz-bearing lithologies. However, in view of the well-established, routinely and widely performed analyses of ^{10}Be, in most cases ^{10}Be dating will be preferred over *in situ* ^{14}C for studying fault scarps in silicate rocks. On the other hand when combined with ^{10}Be, *in situ* ^{14}C offers a substantial benefit for more accurate exposure dating of older fault planes because the *in situ* ^{14}C concentration measured in a saturated surface allows the direct determination of the amount surface erosion on the dated surfaces.

6. Synthesis

Current abilities in *in situ* cosmogenic ^{14}C analysis have introduced new prospects for reconstructing complex surface exposure histories, in particular complex glacier chronologies on the Late Pleistocene to Holocene timescale, and the quantification of geomorphologic process rates. Results from the studies performed in different glacial settings demonstrate that combining analyses of the short-lived *in situ* ^{14}C nuclide with those of ^{10}Be (and ^{26}Al) improves the temporal resolution and hence provides better-constrained glacial histories. This provides unique opportunities to study the evolution of previously glaciated ancient landscapes that have been preserved under non-erosive, cold-based ice through several glacial-interglacial cycles. The absence of inheritance for *in situ* ^{14}C also gives a minimum estimate for the time span of local glaciation which is given by the time needed for *in situ* ^{14}C to decay to near-zero levels while shielded under thick glacier ice.

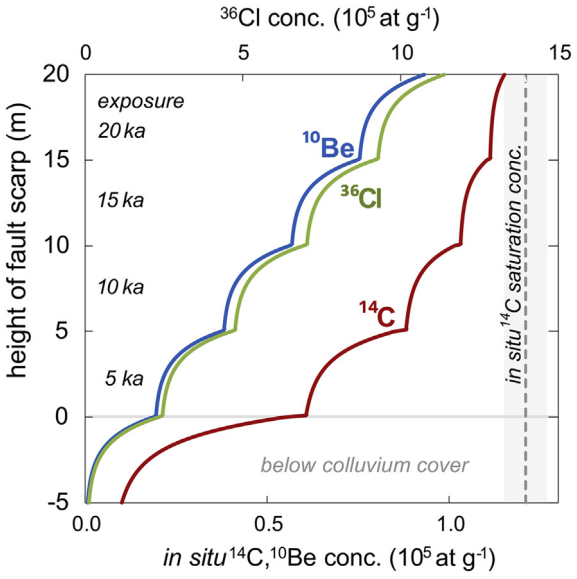

Fig. 16. Synthetic profiles showing the theoretical distribution of the ^{36}Cl, ^{10}Be and *in situ* ^{14}C concentrations along a fault scarp exposed during 5 m displacement events at 5 ka intervals (for a detailed discussion see Benedetti et al., 2002; Akcar et al., 2012; Tikhomirov et al., 2014). A fault plane angle of 45°, horizontal colluvium cover, a bedrock density of 2.65 g cm^{-3} and a density of the colluvium of 1.4 g cm^{-3} were used. For simplicity, exponential depth dependence was assumed for spallogenic and muonic nuclide production. Scaling factors for self-shielding of the scarp plane were derived from Dunne et al. (1999). Note the rapid approach of the *in situ* ^{14}C concentration to the saturation level (given here with a 5% uncertainty interval) with increasing exposure age and scarp height. The rapid increase in the *in situ* ^{14}C concentration below the colluvial cover is due to the overall higher *in situ* ^{14}C production rate compared to ^{10}Be as well as the larger contribution by muonic production.

Studies from the European Alps have demonstrated that the *in situ* ^{14}C-^{10}Be chronometer can constrain the timing and duration of Holocene glacier readvances and assess the impact of Holocene climate variability on high Alpine glacier systems. The high sensitivity of the *in situ* ^{14}C-^{10}Be pair even to limited surface shielding can provide additional constraints on environmental parameters, e.g. the amount of local snow cover during the Holocene. Moreover, in recently exposed surfaces with a well-constrained exposure-burial history the measured *in situ* ^{14}C and ^{10}Be can also be combined to calculate subglacial erosion rates.

With only few studies published so far, applications of *in situ* ^{14}C in sediments and soils remain largely unexplored. A crucial assumption for an accurate interpretation of paired *in situ* ^{14}C-^{10}Be data in fluvial sediments or sedimentary deposits is that the analysed sediment has been in erosion-controlled, isotopic steady-state when leaving the source area. Under this condition, combined *in situ* ^{14}C-^{10}Be analysis in fluvial systems constitutes an effective tracer of sediment transfer times on timescales of 10^3–10^4 years. This covers the typical duration of sediment storage in many natural systems and bridges the time gap between modern sediment yield data and long-term cosmogenic sediment flux rates obtained from ^{10}Be and ^{26}Al data. The *in situ* ^{14}C-^{10}Be pair further offers different approaches to date young (<25 ka) sedimentary deposits in analogy to ^{26}Al-^{10}Be burial dating and depth profile dating methods. Moreover, it is a singular tool to study landscape transience as it allows detecting changes in surface erosion rates and events of rapid mass removal from the surface, e.g. by climate- and/or human-caused soil stripping. *In situ* ^{14}C might further be used in studies on soil dynamics by quantifying effective soil mixing depths. Moreover, measurements of *in situ* ^{14}C in saturated surfaces (>25 ka exposure) provide a direct estimate on surface erosion allowing more accurate cosmogenic-nuclide surface exposure dating.

In view of the remarkable first results of combined *in situ* ^{14}C-^{10}Be analysis and the need to resolve complex landscape evolution in more detail, *in situ* ^{14}C could contribute increasingly to cosmogenic nuclide applications in Earth surface sciences. To exploit its full potential, future development needs to advance the current analytical techniques in order to increase the reliability of *in situ* ^{14}C analyses. The most relevant tasks are i) to improve the analytical reproducibility, ii) reduce the background level, and iii) to refine the *in situ* ^{14}C production rate calibration, notably for muonic production. Recent improvements made in the automation of the extraction process seem most promising for improving the reproducibility to well below the 6.3% found in the CRONUS inter-laboratory comparison. This will be an important step towards a higher sensitivity for very short burial times of only a few hundred years, for example in the context of LIA glacier readvances or for dating young sedimentary deposits. A reduction of the blank level is most important for low concentration measurements, i.e. in the study of very recently exposed rock surfaces for which the blank correction contributes significantly to the total analytical uncertainty as well as any measurements of samples from depth profiles. Currently achieved blank levels range over one order of magnitude with lowest blanks derived from extraction systems that do not employ a flux agent in the extraction process. Minimizing the large uncertainties related to the blank correction which mainly reflect the large scatter in the blank analyses, will also prepare the ground for further reliable analyses of muonic *in situ* ^{14}C production at greater depths. With these improvements, the combination of *in situ* ^{14}C analysis with one or more long-lived nuclide could open up further novel opportunities for the use of cosmogenic nuclides to decipher the history of landscape development. Most importantly, simplified and more reliable analytical procedures should lead to a greater accessibility of researchers to *in situ* ^{14}C analyses which is a

prerequisite for an advanced use of *in situ* ^{14}C in the future.

Acknowledgements

The author wishes to thank the many scientists and technicians that have contributed to the *in situ* ^{14}C research performed at ETH Zürich over the past 10 years. Many thanks to the group of Isotope Geochemistry and to all members of the Laboratory of Ion Beam Physics. Special thanks to F. Kober and L. Wacker for their dedication and encouragement. M. Lupker, S. Ivy-Ochs and R. Wieler are thanked for helpful comments on an earlier version of the manuscript, many valuable discussions and great support. Constructive reviews by N. Akçar and an anonymous reviewer helped to considerably improve the manuscript. The author acknowledges funding by the Swiss National Science Foundation MHV grant (PMPDP2_158288/1).

References

Akcar, N., Ivy-Ochs, S., Kubik, P.W., Schlüchter, C., 2011. Post-depositional impacts on 'Findlinge' (erratic boulders) and their implications for surface-exposure dating. Swiss J. Geosci. 104, 445–453.
Akcar, N., Tikhomirov, D., Ozkaymak, C., Ivy-Ochs, S., Alfimov, V., Sozbilir, H., Uzel, B., Schlüchter, C., 2012. Cl-36 exposure dating of paleoearthquakes in the Eastern Mediterranean: first results from the western Anatolian Extensional Province, Manisa fault zone. Turk. Geol. Soc. Am. Bull. 124, 1724–1735.
Anderson, E.C., Libby, W.F., Weinhouse, S., Reid, A.F., Kirshenbaum, A.D., Grosse, A.V., 1947. Natural radiocarbon from cosmic radiation. Phys. Rev. 72, 931–936.
Anderson, R.K., Miller, G.H., Briner, J.P., Lifton, N.A., DeVogel, S.B., 2008. A millennial perspective on Arctic warming from C-14 in quartz and plants emerging from beneath ice caps. Geophys. Res. Lett. 35, L01502.
Anderson, R.S., Repka, J.L., Dick, G.S., 1996. Explicit treatment of inheritance in dating depositional surfaces using in situ Be-10 and Al-26. Geology 24, 47–51.
Argento, D.C., Stone, J.O., Reedy, R.C., O'Brien, K., 2015a. Physics-based modeling of cosmogenic nuclides part I - Radiation transport methods and new insights. Quat. Geochronol. 26, 29–43.
Argento, D.C., Stone, J.O., Reedy, R.C., O'Brien, K., 2015b. Physics-based modeling of cosmogenic nuclides part II - key aspects of in-situ cosmogenic nuclide production. Quat. Geochronol. 26, 44–55.
Balco, G., 2011. Contributions and unrealized potential contributions of cosmogenic-nuclide exposure dating to glacier chronology, 1990-2010. Quat. Sci. Rev. 30, 3–27.
Balco, G., 2017. Production rate calculations for cosmic-ray-muon-produced Be-10 and Al-26 benchmarked against geological calibration data. Quat. Geochronol. 39, 150–173.
Balco, G., Rovey, C.W., 2008. An isochron method for cosmogenic-nuclide dating of buried soils and sediments. Am. J. Sci. 308, 1083–1114.
Balco, G., Rovey, C.W., Granger, D.E., 2008a. Multiple-cosmogenic-nuclide isochron methods. Geochim. Cosmochim. Acta 72, A47.
Balco, G., Soreghan, G.S., Sweet, D.E., Marra, K.R., Bierman, P.R., 2013. Cosmogenic-nuclide burial ages for Pleistocene sedimentary fill in Unaweep Canyon, Colorado, USA. Quat. Geochronol. 18, 149–157.
Balco, G., Stone, J.O., Lifton, N.A., Dunai, T.J., 2008b. A complete and easily accessible means of calculating surface exposure ages or erosion rates from Be-10 and Al-26 measurements. Quat. Geochronol. 3, 174–195.
Balco, G., Stone, J.O.H., Sliwinski, M.G., Todd, C., 2014. Features of the glacial history of the Transantarctic Mountains inferred from cosmogenic Al-26, Be-10 and Ne-21 concentrations in bedrock surfaces. Antarct. Sci. 26, 708–723.
Beel, C.R., Goehring, B.M., Lifton, N.A., 2015. How many and from where? Assessing the sensitivity of exposure durations calculated from paired bedrock C-14/Be-10 measurements in glacial troughs. Quat. Geochronol. 29, 1–5.
Benedetti, L., Finkel, R., Papanastassiou, D., King, G., Armijo, R., Ryerson, F., Farber, D., Flerit, F., 2002. Post-glacial slip history of the Sparta fault (Greece) determined by Cl-36 cosmogenic dating: evidence for non-periodic earthquakes. Geophys. Res. Lett. 29, 10.1029/2001GL014510.
Berg, S., White, D.A., Bennike, O., Fulop, R.H., Fink, D., Wagner, B., Melles, M., 2016. Unglaciated areas in east Antarctica during the last glacial (marine isotope stage 3) - new evidence from rauer group. Quat. Sci. Rev. 153, 1–10.
Bierman, P.R., Davis, P.T., Corbett, L.B., Lifton, N.A., Finkel, R.C., 2015. Cold-based Laurentide ice covered new England's highest summits during the last glacial maximum. Geology 43, 1059–1062.
Bierman, P.R., Marsella, K.A., Patterson, C., Davis, P.T., Caffee, M., 1999. Mid-Pleistocene cosmogenic minimum-age limits for pre-Wisconsinan glacial surfaces in southwestern Minnesota and southern Baffin island: a multiple nuclide approach. Geomorphology 27, 25–39.
Borchers, B., Marrero, S., Balco, G., Caffee, M., Goehring, B., Lifton, N., Nishiizumi, K., Phillips, F., Schaefer, J., Stone, J., 2016. Geological calibration of spallation production rates in the CRONUS-Earth project. Quat. Geochronol. 31, 188–198.
Braucher, R., Del Castillo, P., Siame, L., Hidy, A.J., Bourles, D.L., 2009. Determination of both exposure time and denudation rate from an in situ-produced Be-10 depth profile: a mathematical proof of uniqueness. Model sensitivity and applications to natural cases. Quat. Geochronol. 4, 56–67.
Briner, J.P., Gosse, J.C., Bierman, P.R., 2006. Applications of cosmogenic nuclides to Laurentide ice sheet history and dynamics. Geol. Soc. Am. Spec. Pap. 415, 29–41.
Briner, J.P., Lifton, N.A., Miller, G.H., Refsnider, K., Anderson, R., Finkel, R., 2014. Using in situ cosmogenic Be-10, C-14, and Al-26 to decipher the history of polythermal ice sheets on Baffin Island, Arctic Canada. Quat. Geochronol. 19, 4–13.
Briner, J.P., Swanson, T.W., 1998. Using inherited cosmogenic Cl-36 to constrain glacial erosion rates of the Cordilleran ice sheet. Geology 26, 3–6.
Brown, E.T., Stallard, R.F., Larsen, M.C., Raisbeck, G.M., Yiou, F., 1995. Denudation rates determined from the accumulation of in situ-produced Be-10 in the Luquillo experimental forest, Puerto-rico. Earth Planet. Sci. Lett. 129, 193–202.
Caffee, M.W., Nishiizumi, K., Sisterson, J.M., Ullmann, J., Welten, K.C., 2013. Cross section measurements at neutron energies 71 and 112 MeV and energy integrated cross section measurements (0.1 < E-n < 750 MeV) for the neutron induced reactions O(n,x)Be-10, Si(n,x)Be-10, and Si(n,x)Al-26. Nucl. Instrum. Methods Phys. Res. B 294, 479–483.
Cerling, T.E., Craig, H., 1994. Geomorphology and in-situ cosmogenic isotopes. Ann. Rev. Earth Planet. Sci. 22, 273–317.
Ciner, A., Dogan, U., Yildirim, C., Akcar, N., Ivy-Ochs, S., Alfimov, V., Kubik, P.W., Schlüchter, C., 2015. Quaternary uplift rates of the Central Anatolian Plateau, Turkey: insights from cosmogenic isochron-burial nuclide dating of the Kizilirmak River terraces. Quat. Sci. Rev. 107, 81–97.
Corbett, L.B., Bierman, P.R., Graly, J.A., Neumann, T.A., Rood, D.H., 2013. Constraining landscape history and glacial erosivity using paired cosmogenic nuclides in Upernavik, northwest Greenland. Geol. Soc. Am. Bull. 125, 1539–1553.
Cresswell, R.G., Beukens, R.P., Rucklidge, J.C., Miura, Y., 1994. Distinguishing spallogenic from non-spallogenic carbon in chondrites using gas and temperature separations. Nucl. Instrum. Methods Phys. Res. B 92, 505–509.
Cresswell, R.G., Miura, Y., Beukens, R.P., Rucklidge, J.C., 1993. 14C terrestrial ages of nine Antarctic meteorites using CO and CO2 temperature extractions. Proc. NIPR Symposium Antarct. Meteorites 6, 381–390.
Davis, P.T., Briner, J.P., Coulthard, R.D., Finkel, R.W., Miller, G.H., 2006. Preservation of Arctic landscapes overridden by cold-based ice sheets. Quat. Res. 65, 156–163.
Desilets, D., Zreda, M., 2003. Spatial and temporal distribution of secondary cosmic-ray nucleon intensities and applications to in situ cosmogenic dating. Earth Planet. Sci. Lett. 206, 21–42.
Desilets, D., Zreda, M., Prabu, T., 2006. Extended scaling factors for in situ cosmogenic nuclides: new measurements at low latitude. Earth Planet. Sci. Lett. 246, 265–276.
Desmarais, D., 1978a. Carbon, nitrogen and sulphur in Apollo 15, 16 and 17 rocks. Proceedings of the 9th Lunar and Planetary Science Conference, 2451-2467.
Desmarais, D.J., 1978b. Variable-temperature cryogenic trap for separation of gas-mixtures. Anal. Chem. 50, 1405–1406.
Desmarais, D.J., Moore, J.G., 1984. Carbon and its isotopes in mid-oceanic basaltic glasses. Earth Planet. Sci. Lett. 69, 43–57.
Di Nicola, L., Strasky, S., Schlüchter, C., Salvatore, M.C., Kubik, P.W., Ivy-Ochs, S., Wieler, R., Akcar, N., Baroni, C., 2007. Complex Exposure History of Pre-LGM Glacial Drifts in Terra Nova Bay, Victoria Land, Using a Multiple Cosmogenic Nuclide Approach. U.S. Geological Survey and The National Academies. USGS OF-2007-1047, Extended Abstract 120.
Dühnforth, M., Anderson, R.S., Ward, D., Stock, G.M., 2010. Bedrock fracture control of glacial erosion processes and rates. Geology 38, 423–426.
Dunai, T.J., 2001a. Influence of secular variation of the geomagnetic field on production rates of in situ produced cosmogenic nuclides. Earth Planet. Sci. Lett. 193, 197–212.
Dunai, T.J., 2001b. Reply to comment on 'Scaling factors for production rates of in situ produced cosmogenic nuclides: a critical reevaluation' by Darin Desilets, Marek Zreda and Nathaniel Lifton. Earth Planet. Sci. Lett. 188, 289–298.
Dunai, T.J., 2010. Cosmogenic Nuclides, Principles, Concepts and Applications in the Earth Surface Sciences. Cambridge University Press.
Dunne, J., Elmore, D., Muzikar, P., 1999. Scaling factors for the rates of production of cosmogenic nuclides for geometric shielding and attenuation at depth on sloped surfaces. Geomorphology 27, 3–11.
Dyke, A.S., Andrews, J.T., Clark, P.U., England, J.H., Miller, G.H., Shaw, J., Veillette, J.J., 2002. The Laurentide and innuitian ice sheets during the last glacial maximum. Quat. Sci. Rev. 21, 9–31.
Dyke, A.S., Prest, V.K., 1987. Late wisconsinan and Holocene history of the Laurentide ice sheet. Géogr. physique Quaternaire XLI (n°2), 237–263.
Ehlers, J., Gibbard, P.L., Hughes, P.D., 2011. Quaternary glaciations - extent and chronology a closer Look introduction. Dev. Quat. Sci. 15, 1–14.
Erlanger, E.D., Granger, D.E., Gibbon, R.J., 2012. Rock uplift rates in South Africa from isochron burial dating of fluvial and marine terraces. Geology 40, 1019–1022.
Fabel, D., Fink, D., Fredin, O., Harbor, J., Land, M., Stroeven, A.P., 2006. Exposure ages from relict lateral moraines overridden by the Fennoscandian ice sheet. Quat. Res. 65, 136–146.
Fabel, D., Stroeven, A.P., Harbor, J., Kleman, J., Elmore, D., Fink, D., 2002. Landscape preservation under Fennoscandian ice sheets determined from in situ produced Be-10 and Al-26. Earth Planet. Sci. Lett. 201, 397–406.
Fogwill, C.J., Turney, C.S.M., Golledge, N.R., Rood, D.H., Hippe, K., Wacker, L., Wieler, R., Rainsley, E.B., Jones, R.S., 2014. Drivers of abrupt Holocene shifts in West Antarctic ice stream direction determined from combined ice sheet modelling and geologic signatures. Antarct. Sci. 26, 674–686.
Fülöp, R.H., Bishop, P., Fabel, D., Cook, G.T., Everest, J., Schnabel, C., Codilean, A.T.,

Xu, S., 2015a. Quantifying soil loss with in-situ cosmogenic Be-10 and C-14 depth-profiles. Quat. Geochronol. 27, 78–93.
Fülöp, R.H., Naysmith, P., Cook, G.T., Fabel, D., Xu, S., Bishop, P., 2010. Update on the performance of the Suerc in situ cosmogenic C-14 extraction line. Radiocarbon 52, 1288–1294.
Fülöp, R.H., Wacker, L., Dunai, T.J., 2015b. Progress report on a novel in situ C-14 extraction scheme at the University of Cologne. Nucl. Instrum. Methods Phys. Res. B 361, 20–24.
Gjermundsen, E.F., Briner, J.P., Akcar, N., Foros, J., Kubik, P.W., Salvigsen, O., Hormes, A., 2015. Minimal erosion of Arctic alpine topography during late Quaternary glaciation. Nat. Geosci. 8, 789–793.
Glasser, N.F., Hughes, P.D., Fenton, C., Schnabel, C., Rother, H., 2012. 10Be and 26Al exposure-age dating of bedrock surfaces on the aran ridge, wales: evidence for a thick welsh ice cap at the last glacial maximum. J. Quat. Sci. 27, 97–104.
Goehring, B.M., Muzikar, P., Lifton, N.A., 2013. An in situ C-14-Be-10 Bayesian isochron approach for interpreting complex glacial histories. Quat. Geochronol. 15, 61–66.
Goehring, B.M., Schaefer, J.M., Schluechter, C., Lifton, N.A., Finkel, R.C., Jull, A.J.T., Akcar, N., Alley, R.B., 2011. The Rhone Glacier was smaller than today for most of the Holocene. Geology 39, 679–682.
Goehring, B.M., Schimmelpfennig, I., Schaefer, J.M., 2014. Capabilities of the Lamont-Doherty Earth Observatory in situ C-14 extraction laboratory updated. Quat. Geochronol. 19, 194–197.
Goel, P.S., Kohman, T.P., 1962. Cosmogenic Carbon-14 in meteorites and terrestrial ages of finds and craters. Science 136, 875–876.
Gosse, J.C., Phillips, F.M., 2001. Terrestrial in situ cosmogenic nuclides: theory and application. Quat. Sci. Rev. 20, 1475–1560.
Granger, D.E., 2006. A review of burial dating methods using 26Al and 10Be. Geol. Soc. Am. Spec. Pap. 415, 1–16.
Granger, D.E., 2014. 14.7-Cosmogenic nuclide burial dating in archaeology and Paleoanthropology a2-Holland. In: Heinrich, D., Turekian, K.K. (Eds.), Treatise on Geochemistry, second ed. Elsevier, Oxford, pp. 81–97.
Granger, D.E., Gibbon, R.J., Kuman, K., Clarke, R.J., Bruxelles, L., Caffee, M.W., 2015. New cosmogenic burial ages for Sterkfontein member 2 australopithecus and member 5 oldowan. Nature 522, 85–U200.
Granger, D.E., Lifton, N.A., Willenbring, J.K., 2013. A cosmic trip: 25 years of cosmogenic nuclides in geology. Geol. Soc. Am. Bull. 125, 1379–1402.
Granger, D.E., Muzikar, P.F., 2001. Dating sediment burial with in situ-produced cosmogenic nuclides: theory, techniques, and limitations. Earth Planet. Sci. Lett. 188, 269–281.
Granger, D.E., Riebe, C.S., 2007. Cosmogenic nuclides in weathering and erosion. In: Holland, H.D., Turekian, K.K. (Eds.), Treatise on Geochemistry, 2 ed. Elsevier, Amsterdam, pp. 1–43.
Granger, D.E., Smith, A.L., 2000. Dating buried sediments using radioactive decay and muogenic production of Al-26 and Be-10. Nucl. Instrum. Methods Phys. Res. B 172, 822–826.
Hallet, B., Hunter, L., Bogen, J., 1996. Rates of erosion and sediment evacuation by glaciers: a review of field data and their implications. Glob. Planet Change 12, 213–235.
Handwerger, D.A., Cerling, T.E., Bruhn, R.L., 1999. Cosmogenic C-14 in carbonate rocks. Geomorphology 27, 13–24.
Harbor, J., Stroeven, A.P., Fabel, D., Clarhall, A., Kleman, J., Li, Y.K., Elmore, D., Fink, D., 2006. Cosmogenic nuclide evidence for minimal erosion across two subglacial sliding boundaries of the late glacial Fennoscandian ice sheet. Geomorphology 75, 90–99.
Harrington, C.D., Whitney, J.W., Jull, A.J.T., Phillips, W., 2000. Cosmogenic Dating and Analysis of Scarps along the Solitario Canyon and Windy Wash Faults, Yucca Mountain, Nevada, Geologic and Geophysical Characterization Studies of Yucca Mountain, Nevada. U.S. Geological Survey Digital Data Series 58, 9 pp..
Hein, A.S., Fogwill, C.J., Sugden, D.E., Xu, S., 2014. Geological scatter of cosmogenic-nuclide exposure ages in the Shackleton Range, Antarctica: implications for glacial history. Quat. Geochronol. 19, 52–66.
Heisinger, B., Lal, D., Jull, A.J.T., Kubik, P., Ivy-Ochs, S., Knie, K., Nolte, E., 2002a. Production of selected cosmogenic radionuclides by muons: 2. Capture of negative muons. Earth Planet. Sci. Lett. 200, 357–369.
Heisinger, B., Lal, D., Jull, A.J.T., Kubik, P., Ivy-Ochs, S., Neumaier, S., Knie, K., Lazarev, V., Nolte, E., 2002b. Production of selected cosmogenic radionuclides by muons 1. Fast muons. Earth Planet. Sci. Lett. 200, 345–355.
Heisinger, B., Nolte, E., 2000. Cosmogenic in situ production of radionuclides: exposure ages and erosion rates. Nucl. Instrum. Methods Phys. Res. B 172, 790–795.
Heyman, J., Stroeven, A.P., Harbor, J.M., Caffee, M.W., 2011. Too young or too old: evaluating cosmogenic exposure dating based on an analysis of compiled boulder exposure ages. Earth Planet. Sci. Lett. 302, 71–80.
Hidy, A.J., Gosse, J.C., Pederson, J.L., Mattern, J.P., Finkel, R.C., 2010. A geologically constrained Monte Carlo approach to modeling exposure ages from profiles of cosmogenic nuclides: an example from Lees Ferry, Arizona. Geochem. Geophys. Geosys 11. http://dx.doi.org/10.1029/2010GC003084.
Hildes, D.H.D., Clarke, G.K.C., Flowers, G.E., Marshall, S.J., 2004. Subglacial erosion and englacial sediment transport modelled for North American ice sheets. Quat. Sci. Rev. 23, 409–430.
Hippe, K., Ivy-Ochs, S., Kober, F., Zasadni, J., Wieler, R., Wacker, L., Kubik, P.W., Schlüchter, C., 2014. Chronology of Lateglacial ice flow reorganization and deglaciation in the Gotthard Pass area, Central Swiss Alps, based on cosmogenic Be-10 and in situ C-14. Quat. Geochronol. 19, 14–26.
Hippe, K., Kober, F., Baur, H., Ruff, M., Wacker, L., Wieler, R., 2009. The current performance of the in situ C-14 extraction line at ETH. Quat. Geochronol 4, 493–500.
Hippe, K., Kober, F., Ivy-Ochs, S., Lupker, M., Wacker, L., Christl, M., Wieler, R., 2013a. Complex in Situ Cosmogenic 10Be-14C Data Suggest Mid-holocene Climate Change on the Bolivian Altiplano. Goldschmidt2013 Conference Abstracts.
Hippe, K., Kober, F., Wacker, L., Fahrni, S.M., Ivy-Ochs, S., Akcar, N., Schlüchter, C., Wieler, R., 2013b. An update on in situ cosmogenic C-14 analysis at ETH Zurich. Nucl. Instrum. Methods Phys. Res. B 294, 81–86.
Hippe, K., Kober, F., Zeilinger, G., Ivy-Ochs, S., Maden, C., Wacker, L., Kubik, P.W., Wieler, R., 2012. Quantifying denudation rates and sediment storage on the eastern Altiplano, Bolivia, using cosmogenic Be-10, Al-26, and in situ C-14. Geomorphology 179, 58–70.
Hippe, K., Lifton, N.A., 2014. Calculating isotope ratios and nuclide concentrations for in situ cosmogenic C-14 analyses. Radiocarbon 56, 1167–1174.
Hippolyte, J.C., Brocard, G., Tard, M., Nicoud, G., Bourles, D., Braucher, R., Menard, G., Souffache, B., 2006. The recent fault scarps of the Western Alps (France): tectonic surface ruptures or gravitational sackung scarps? A combined mapping, geomorphic, levelling, and Be-10 dating approach. Tectonophysics 418, 255–276.
Ivy-Ochs, S., Briner, J.P., 2014. Dating disappearing ice with cosmogenic nuclides. Elements 10, 351–356.
Ivy-Ochs, S., Kerschner, H., Maisch, M., Christl, M., Kubik, P.W., Schlüchter, C., 2009. Latest Pleistocene and Holocene glacier variations in the european Alps. Quat. Sci. Rev. 28, 2137–2149.
Ivy-Ochs, S., Kerschner, H., Reuther, A., Maisch, M., Sailer, R., Schaefer, J., Kubik, P.W., Synal, H.A., Schlüchter, C., 2006. The timing of glacier advances in the northern European Alps based on surface exposure dating with cosmogenic Be-10, Al-26, Cl-36, and Ne-21. Geol. Soc. Am. Spec. Pap. 415, 43–60.
Ivy-Ochs, S., Kerschner, H., Schlüchter, C., 2007. Cosmogenic nuclides and the dating of Lateglacial and Early Holocene glacier variations: the Alpine perspective. Quat. Int. 164–65, 53–63.
Jerolmack, D.J., Paola, C., 2010. Shredding of environmental signals by sediment transport. Geophys. Res. Lett. 37, L19401.
Jull, A.J.T., Burr, G.S., 2006. Accelerator mass spectrometry: is the future bigger or smaller? Earth Planet. Sci. Lett. 243, 305–325.
Jull, A.J.T., Donahue, D.J., Linick, T.W., Wilson, G.C., 1989. Spallogenic C-14 in high-altitude rocks and in antarctic meteorites. Radiocarbon 31, 719–724.
Jull, A.J.T., Lifton, N., Phillips, W.M., Quade, J., 1994. Studies of the production-rate of cosmic-ray produced C-14 in rock surfaces. Nucl. Instrum. Methods Phys. Res. B 92, 308–310.
Jull, A.J.T., Scott, E.M., Bierman, P., 2015. The CRONUS-Earth inter-comparison for cosmogenic isotope analysis. Quat. Geochronol. 26, 3–10.
Jull, A.J.T., Wilson, A.E., Burr, G.S., Toolin, L.J., Donahue, D.J., 1992. Measurements of cosmogenic C-14 produced by spallation in high-altitude rocks. Radiocarbon 34, 737–744.
Kelly, M.A., Ivy-Ochs, S., Kubik, P.W., von Blanckenburg, F., Schlüchter, C., 2006. Chronology of deglaciation based on Be-10 dates of glacial erosional features in the Grimsel Pass region, central Swiss Alps. Boreas 35, 634–643.
Kim, D.E., Seong, Y.B., Byun, J., Weber, J., Min, K.W., 2016. Geomorphic disequilibrium in the Eastern Korean Peninsula: possible evidence for reactivation of a rift-flank margin. Geomorphology 254, 130–145.
Kim, K.J., Lal, D., Englert, P.A.J., Southon, J., 2007. In situ C-14 depth profile of subsurface vein quartz samples from Macraes Flat New Zealand. Nucl. Instrum. Methods Phys. Res. B 259, 632–636.
Kleman, J., 1994. Preservation of landforms under-ice sheets and ice caps. Geomorphology 9, 19–32.
Kleman, J., Glasser, N.F., 2007. The subglacial thermal organisation (STO) of ice sheets. Quat. Sci. Rev. 26, 585–597.
Kleman, J., Hättestrand, C., 1999. Frozen-bed fennoscandian and Laurentide ice sheets during the last glacial maximum. Nature 402, 63–66.
Kober, F., Hippe, K., Salcher, B., Ivy-Ochs, S., Kubik, P.W., Wacker, L., Hählen, N., 2012. Debris-flow-dependent variation of cosmogenically derived catchment-wide denudation rates. Geology 40, 935–938.
Kong, P., Fink, D., Na, C.G., Xiao, W., 2010. Dip-slip rate determined by cosmogenic surface dating on a Holocene scarp of the Daju fault, Yunnan, China. Tectonophysics 493, 106–112.
Lal, D., 1988. Insitu - produced cosmogenic isotopes in terrestrial rocks. Ann. Rev. Earth Planet. Sci. 16, 355–388.
Lal, D., 1991. Cosmic-ray Labeling of erosion surfaces - insitu nuclide production-rates and erosion models. Earth Planet. Sci. Lett. 104, 424–439.
Lal, D., Jull, A.J.T., 1994. Studies of cosmogenic in-situ (Co)-C-14 and (Co2)-C-14 produced in terrestrial and extraterrestrial samples - experimental procedures and applications. Nucl. Instrum. Methods Phys. Res. B 92, 291–296.
Lal, D., Jull, A.J.T., 2001. In-situ cosmogenic C-14: production and examples of its unique applications in studies of terrestrial and extraterrestrial processes. Radiocarbon 43, 731–742.
Lal, D., Pavich, M., Gu, Z.Y., Jull, A.J.T., Caffee, M., Finkel, R., Southon, J., 1996. Recent erosional history of a soil profile based on cosmogenic in-situ radionuclides 14C and 10Be. Earth processes: reading the isotopic code. Geophys. Monogr. 95, 371–377.
Lal, D., Peters, B., 1967. Cosmic-ray produced radioactivity on the earth. In: Flugge, S. (Ed.), Handbuch der Physik. Springer Verlag, Berlin, pp. 551–612.
Lauer, J.W., Willenbring, J., 2010. Steady state reach-scale theory for radioactive tracer concentration in a simple channel/floodplain system. J. Geophys. Res.-

Earth 115, F04018. http://dx.doi.org/10.1029/2009JF001480.
Li, Y.K., Fabel, D., Stroeven, A.P., Harbor, J., 2008. Unraveling complex exposure-burial histories of bedrock surfaces under ice sheets by integrating cosmogenic nuclide concentrations with climate proxy records. Geomorphology 99, 139–149.
Libby, W.F., 1946. Atmospheric Helium three and radiocarbon from cosmic radiation. Phys. Rev. 69, 671–672.
Libby, W.F., Anderson, E.C., Arnold, J.R., 1949. Age determination by radiocarbon content - world-wide assay of natural radiocarbon. Science 109, 227–228.
Lifton, N., Goehring, B., Wilson, J., Kubley, T., Caffee, M., 2015. Progress in automated extraction and purification of in situ C-14 from quartz: results from the Purdue in situ C-14 laboratory. Nucl. Instrum. Methods Phys. Res. B 361, 381–386.
Lifton, N., Sato, T., Dunai, T.J., 2014. Scaling in situ cosmogenic nuclide production rates using analytical approximations to atmospheric cosmic-ray fluxes. Earth Planet. Sci. Lett. 386, 149–160.
Lifton, N., Smart, D.F., Shea, M.A., 2008. Scaling time-integrated in situ cosmogenic nuclide production rates using a continuous geomagnetic model. Earth Planet. Sci. Lett. 268, 190–201.
Lifton, N.A., Bieber, J.W., Clem, J.M., Duldig, M.L., Evenson, P., Humble, J.E., Pyle, R., 2005. Addressing solar modulation and long-term uncertainties in scaling secondary cosmic rays for in situ cosmogenic nuclide applications. Earth Planet. Sci. Lett. 239, 140–161.
Lifton, N.A., Jull, A.J.T., Quade, J., 2001. A new extraction technique and production rate estimate for in situ cosmogenic C-14 in quartz. Geochim. Cosmochim. Acta 65, 1953–1969.
Lupker, M., Hippe, K., Wacker, L., Kober, F., Maden, C., Braucher, R., Bourles, D., Romani, J.R.V., Wieler, R., 2015. Depth-dependence of the production rate of in situ C-14 in quartz from the Leymon High core, Spain. Quat. Geochronol. 28, 80–87.
Marrero, S.M., Phillips, F.M., Borchers, B., Lifton, N., Aumer, R., Balco, G., 2016. Cosmogenic nuclide systematics and the CRONUScalc program. Quat. Geochronol. 31, 160–187.
Marshall, S.J., James, T.S., Clarke, G.K.C., 2002. North american ice sheet reconstructions at the last glacial maximum. Quat. Sci. Rev. 21, 175–192.
Martin, L.C.P., Blard, P.H., Balco, G., Lavé, J., Delunel, R., Lifton, N., Laurent, V., 2017. The CREp program and the ICE-D production rate calibration database: a fully parameterizable and updated online tool to compute cosmic-ray exposure ages. Quat. Geochronol. 38, 25–49.
Masarik, J., Frank, M., Schafer, J.M., Wieler, R., 2001. Correction of in situ cosmogenic nuclide production rates for geomagnetic field intensity variations during the past 800,000 years. Geochim. Cosmochim. Acta 65, 2995–3003.
Matmon, A., Hidy, A.J., Vainer, S., Crouvi, O., Fink, D., Erel, Y., Horwitz, L.K., Chazan, M., Team, A., 2015. New chronology for the southern Kalahari Group sediments with implications for sediment-cycle dynamics and early hominin occupation. Quat. Res. 84, 118–132.
Matmon, A., Nichols, K., Finkel, R., 2006. Isotopic insights into smoothening of abandoned fan surfaces, Southern California. Quat. Res. 66, 109–118.
Miller, G.H., Briner, J.P., Lifton, N.A., Finkel, R.C., 2006. Limited ice-sheet erosion and complex in situ cosmogenic Be-10, Al-26, and C-14 on Baffin Island, Arctic Canada. Quat. Geochronol. 1, 74–85.
Miller, G.H., Wolfe, A.P., Steig, E.J., Sauer, P.E., Kaplan, M.R., Briner, J.P., 2002. The Goldilocks dilemma: big ice, little ice, or "just-right" ice in the Eastern Canadian Arctic. Quat. Sci. Rev. 21, 33–48.
Mitchell, S.G., Matmon, A., Bierman, P.R., Enzel, Y., Caffee, M., Rizzo, D., 2001. Displacement history of a limestone normal fault scarp, northern Israel, from cosmogenic Cl-36. J. Geophys. Res.-Sol Ea. 106, 4247–4264.
Mudd, S.M., 2016. Detection of transience in eroding landscapes. Earth Surf. Proc. Land 42, 24–41.
National Nuclear Data Center, B.N.L., www.nndc.bnl.gov.
Navrotsky, A., 1994. Thermochemistry of crystalline and amorphous Silica. Rev. Mineral. 29, 309–329.
Naysmith, P., Cook, G.T., Phillips, W.M., Lifton, N.A., Anderson, R., 2004. Preliminary results for the extraction and measurement of cosmogenic in situ C-14 from quartz. Radiocarbon 46, 201–206.
Nesje, A., Dahl, S.O., Valen, V., Øvstedal, J., 1992. Quaternary erosion in the Sognefjord drainage basin, western Norway. Geomorphology 5, 511–520.
Nishiizumi, K., Winterer, E.L., Kohl, C.P., Klein, J., Middleton, R., Lal, D., Arnold, J.R., 1989. Cosmic-ray production-rates of Be-10 and Al-26 in quartz from glacially polished rocks. J. Geophys. Res.-Solid 94, 17907–17915.
Phillips, F.M., Argento, D.C., Balco, G., Caffee, M.W., Clem, J., Dunai, T.J., Finkel, R., Goehring, B., Gosse, J.C., Hudson, A.M., Jull, A.J.T., Kelly, M.A., Kurz, M., Lal, D., Lifton, N., Marrero, S.M., Nishiizumi, K., Reedy, R.C., Schaefer, J., Stone, J.O.H., Swanson, T., Zreda, M.G., 2016a. The CRONUS-Earth Project: a synthesis. Quat. Geochronol. 31, 119–154.
Phillips, F.M., Argento, D.C., Bourles, D.L., Caffee, M.W., Dunai, T.J., Goehring, B., Gosse, J.C., Hudson, A.M., Jull, A.J.T., Kelly, M., Lifton, N., Marrero, S.M., Nishiizumi, K., Reedy, R.C., Stone, J.O.H., 2016b. Where now? Reflections on future directions for cosmogenic nuclide research from the CRONUS projects. Quat. Geochronol. 31, 155–159.
Phillips, F.M., Stone, W.D., Fabryka-Martin, J.T., 2001. An improved approach to calculating low-energy cosmic-ray neutron fluxes near the land/atmosphere interface. Chem. Geol. 175, 689–701.
Phillips, J., 2003. Alluvial storage and the long-term stability of sediment yields. Basin Res. 15, 153–163.
Pigati, J.S., Lifton, N.A., Jull, A.J.T., Quade, J., 2010. A simplified in situ cosmogenic C-14 extraction system. Radiocarbon 52, 1236–1243.
Putkonen, J., Swanson, T., 2003. Accuracy of cosmogenic ages for moraines. Quat. Res. 59, 255–261.
Reedy, R.C., 2013. Cosmogenic-nuclide production rates: reaction cross section update. Nucl. Instrum. Methods Phys. Res. B 294, 470–474.
Repka, J.L., Anderson, R.S., Finkel, R.C., 1997. Cosmogenic dating of fluvial terraces, Fremont River. Utah. Earth Planet. Sci. Lett. 152, 59–73.
Riihimaki, C.A., MacGregor, K.R., Anderson, R.S., Anderson, S.P., Loso, M.G., 2005. Sediment evacuation and glacial erosion rates at a small alpine glacier. J. Geophys. Res. - Earth Surf. 110 http://dx.doi.org/10.1029/2004JF000189. F03003.
Ruff, M., Wacker, L., Gaggeler, H.W., Suter, M., Synal, H.A., Szidat, S., 2007. A gas ion source for radiocarbon measurements at 200 kV. Radiocarbon 49, 307–314.
Schaller, M., Ehlers, T.A., Blum, J.D., Kallenberg, M.A., 2009. Quantifying glacial moraine age, denudation, and soil mixing with cosmogenic nuclide depth profiles. J. Geophys. Res.-Earth 114, F01012. http://dx.doi.org/10.1029/2007JF000921.
Schimmelpfennig, I., Schaefer, J.M., Goehring, B.M., Lifton, N., Putnam, A.E., Barrell, D.J.A., 2012. Calibration of the in situ cosmogenic 14C production rate in New Zealand's Southern Alps. J. Quat. Sci. 27, 671–674.
Schlagenhauf, A., Manighetti, I., Benedetti, L., Gaudemer, Y., Finkel, R., Malavieille, J., Pou, K., 2011. Earthquake supercycles in Central Italy, inferred from Cl-36 exposure dating. Earth Planet. Sci. Lett. 307, 487–500.
Stone, J.O., 2000. Air pressure and cosmogenic isotope production. J. Geophys. Res.-Sol Ea. 105, 23753–23759.
Stone, J.O., Balco, G.A., Sugden, D.E., Caffee, M.W., Sass, L.C., Cowdery, S.G., Siddoway, C., 2003. Holocene deglaciation of marie Byrd land, west Antarctica. Science 299, 99–102.
Stroeven, A.P., Fabel, D., Harbor, J., Hättestrand, C., Kleman, J., 2002. Quantifying the erosional impact of the Fennoscandian ice sheet in the Tornetrask-Narvik corridor, northern Sweden, based on cosmogenic radionuclide data. Geogr. Ann. A 84a, 275–287.
Stroeven, A.P., Fabel, D., Harbor, J.M., Fink, D., Caffee, M.W., Dahlgren, T., 2011. Importance of sampling across an assemblage of glacial landforms for interpreting cosmogenic ages of deglaciation. Quat. Res. 76, 148–156.
Stuart, F.M., Dunai, T.J., 2009. Advances in cosmogenic isotope research from Cronus-Eu. Quat. Geochronol. 4, 435–436.
Suess, H.E., Wänke, H., 1962. Radiocarbon content and terrestrial age of 12 Stony meteorites and 1 iron meteorite. Geochim. Cosmochim. Acta 26, 475–480.
Sugden, D.E., Balco, G., Cowdery, S.G., Stone, J.O., Sass, L.C., 2005. Selective glacial erosion and weathering zones in the coastal mountains of Marie Byrd Land, Antarctica. Geomorphology 67, 317–334.
Synal, H.A., Stocker, M., Suter, M., 2007. MICADAS: a new compact radiocarbon AMS system. Nucl. Instrum. Methods Phys. Res. B 259, 7–13.
Tikhomirov, D., Akcar, N., Ivy-Ochs, S., Alfimov, V., Schlüchter, C., 2014. Calculation of shielding factors for production of cosmogenic nuclides in fault scarps. Quat. Geochronol. 19, 181–193.
von Blanckenburg, F., Willenbring, J.K., 2014. Cosmogenic nuclides: dates and rates of earth-surface change. Elements 10, 341–346.
White, D., Fulop, R.H., Bishop, P., Mackintosh, A., Cook, G., 2011. Can in-situ cosmogenic C-14 be used to assess the influence of clast recycling on exposure dating of ice retreat in Antarctica? Quat. Geochronol. 6, 289–294.
Wirsig, C., Ivy-Ochs, S., Akçar, N., Lupker, M., Hippe, K., Wacker, L., Vockenhuber, C., Schlüchter, C., 2016. Combined cosmogenic 10Be, in situ 14C and 36Cl concentrations constrain Holocene history and erosion depth of Grueben glacier (CH). Swiss J. Geosci. 109, 379–388.
Wirsig, C., Ivy-Ochs, S., Reitner, J.M., Christl, M., Vockenhuber, C., Bichler, M., Reindl, M., 2017. Subglacial abrasion rates at Goldbergkees, Hohe Tauern, Austria, determined from cosmogenic 10Be and 36Cl concentrations. Earth Surf. Proc. Land 42, 1119–1131.
Wittmann, H., von Blanckenburg, F., 2009. Cosmogenic nuclide budgeting of floodplain sediment transfer. Geomorphology 109, 246–256.
Yokoyama, Y., Caffee, M.W., Southon, J.R., Nishiizumi, K., 2004. Measurements of in situ produced C-14 in terrestrial rocks. Nucl. Instrum. Methods Phys. Res. B 223, 253–258.
Young, N.E., Briner, J.P., Maurer, J., Schaefer, J.M., 2016. Be-10 measurements in bedrock constrain erosion beneath the Greenland Ice Sheet margin. Geophys. Res. Lett. 43, 11708–11719.
Young, N.E., Schaefer, J.M., Goehring, B., Lifton, N., Schimmelpfennig, I., Briner, J.P., 2014. West Greenland and global in situ C-14 production-rate calibrations. J. Quat. Sci. 29, 401–406.
Zhao, Z.J., Granger, D., Zhang, M.H., Kong, X.G., Yang, S.L., Chen, Y., Hu, E.Y., 2016. A test of the isochron burial dating method on fluvial gravels within the Pulu volcanic sequence, West Kunlun Mountains, China. Quat. Geochronol. 34, 75–80.
Zhao, Z.J., Granger, D.E., Chen, Y., Shu, Q., Liu, G.F., Zhang, M.H., Hu, X.F., Wu, Q.L., Hu, E., Li, Y., Yan, Y.J., Qiao, L.L., 2017. Cosmogenic nuclide burial dating of an alluvial conglomerate sequence: an example from the Hexi Corridor, NE Tibetan Plateau. Quat. Geochronol. 39, 68–78.
Zreda, M., Lifton, N., 2000. Revealing Complex Exposure Histories of Arctic Landforms Using In-situ 14C and 36Cl. AGU, Fall 2000 Meeting, Session U03.
Zreda, M., Noller, J.S., 1998. Ages of prehistoric earthquakes revealed by cosmogenic chlorine-36 in a bedrock fault scarp at Hebgen Lake. Science 282, 1097–1099.